Journal of Sedimentary Research

Journal of Sedimentary Research, 2018, v. 88, 727–742
Research Article
DOI: http://dx.doi.org/10.2110/jsr.2018.37

CALCIUM CARBONATE PRECIPITATION IN DIATOM-RICH MICROBIAL MATS: THE LAGUNA NEGRA HYPERSALINE LAKE, CATAMARCA, ARGENTINA

FERNANDO JAVIER GOMEZ,[1] CECILIA MLEWSKI,[1] FLAVIA JAQUELINA BOIDI,[1]
MARÍA EUGENIA FARÍAS,[2] AND EMMANUELLE GÉRARD[3]

[1]*CICTERRA, Centro de Investigaciones en Ciencias de la Tierra, CONICET-Universidad Nacional de Córdoba, Argentina*
[2]*LIMLA, Laboratorio de Investigaciones Microbiológicas de Lagunas Andinas, Planta Piloto de Procesos Industriales Microbiológicos, CCT, CONICET, Tucumán, Argentina*
[3]*IPGP, Institut de Physique du Globe de Paris, Sorbonne Paris Cité, Université Paris Diderot, CNRS UMR, 7154, 1 rue Jussieu, 75238 Paris cedex 05, France*
e-mail: fjgomez@unc.edu.ar

ABSTRACT: **Carbonate microbialites provide a window to understand microbe–mineral interactions in modern environments and in the geological record. Unraveling microbial versus physicochemical controls and biogeochemical signatures is not always straightforward. Environmental and laboratory studies have shown that microbial activity can play a central role in calcium carbonate precipitation. Most studies have focused on the effects of Bacteria and Archaea activity on carbonate precipitation processes (e.g., cyanobacteria, sulfate-reducing bacteria, sulfide-oxidizing bacteria and iron-reducing bacteria). The influence of eukaryotic activity, such as diatoms and other microalgae, on carbonate precipitation and microbialite formation has been the focus of less attention.**

This study explores carbonate mineralization in active diatom-rich microbial mats developed in a high-altitude groundwater-fed hypersaline lake in the Puna region of Catamarca, Argentina. Previous work has focused on the texture, mineralogy, and stable-isotope chemistry of the subfossil oncoidal and laminar microbialites. Here, using 16S rDNA Bacteria diversity analysis, confocal scanning laser microscopy, scanning electron microscopy, and transmitted-light microscopy, we explore the Bacteria and diatom diversity in the microbial mats and the related carbonates textures and make comparisons with similar textures in the associated oncoidal microbialites. Diatom-rich subspherical aggregates, which have not been previously described in the literature, show a diverse microbial community with abundant exopolymeric substances (EPSs) where carbonate precipitation takes place. These aggregates are a main component of the Laguna Negra microbial mats and show anhedral micritic calcite in the EPS matrix as the main mineral component. Similar calcite micrite textures are also preserved as one lamina type in the associated oncoids. On the other hand, where EPS are absent, carbonate precipitation, related to pennate diatom blooms, is represented by euhedral aragonite needles suggesting different mechanisms and controls. Changes in the microbial communities are recorded in the oncoids as different lamina types, providing a link between the currently active mats and the subfossil oncoidal structures. This is a first survey of these previously unexplored diatom-rich microbial mats developed under extreme environmental conditions in the Laguna Negra. Understanding the effect that the interaction between diatoms and prokaryotic communities has on carbonate precipitation may provide some insight on the evolution of microbialite textures and fabrics, and on the change from prokaryote-dominated systems to mixed eukaryotic–prokaryotic systems.

INTRODUCTION

The mineralized record of microbial life, usually referred to as *microbialites* (Burne and Moore 1987), sheds light on potential microbe–mineral interactions in the geological past. Because of their abundance (Whitman et al. 1998; Kallmeyer et al. 2012) and chemical reactivity (Konhauser 2007), microorganisms play a central role in biogeochemical cycles at both the microscopic and macroscopic scales (Herman and Kump 2005; Falkowski et al. 2008). Microbial life has been pervasive throughout our planet's history (Allwood et al. 2006; Knoll et al. 2016) and has had a significant impact on the evolution of the Earth surface by influencing biogeochemical nutrient cycling (see Canfield et al. 2000, 2006; Catling and Claire 2005) and the precipitation or dissolution of minerals (Banfield et al. 2001; Douglas 2005; Perry et al. 2007). In particular, microbial metabolism can control mineral precipitation, such as the case of carbonates in microbial mats and biofilms (Dupraz and Visscher 2005), the water column (Thompson et al. 1997; Dittrich and Obst 2004), and sediments and pore waters (Soetaert et al. 2007; Schrag et al. 2013). While it is possible to recognize the influence of microbes on various processes in the geological record, differentiating between physicochemical and microbial controls or biogeochemical signatures is not straightforward.

Most studies have focused on the effects of bacterial–archaeal activity on carbonate precipitation processes, mainly cyanobacteria (Arp et al.

Published Online: June 2018
 1527-1404/18/088-727/$03.00

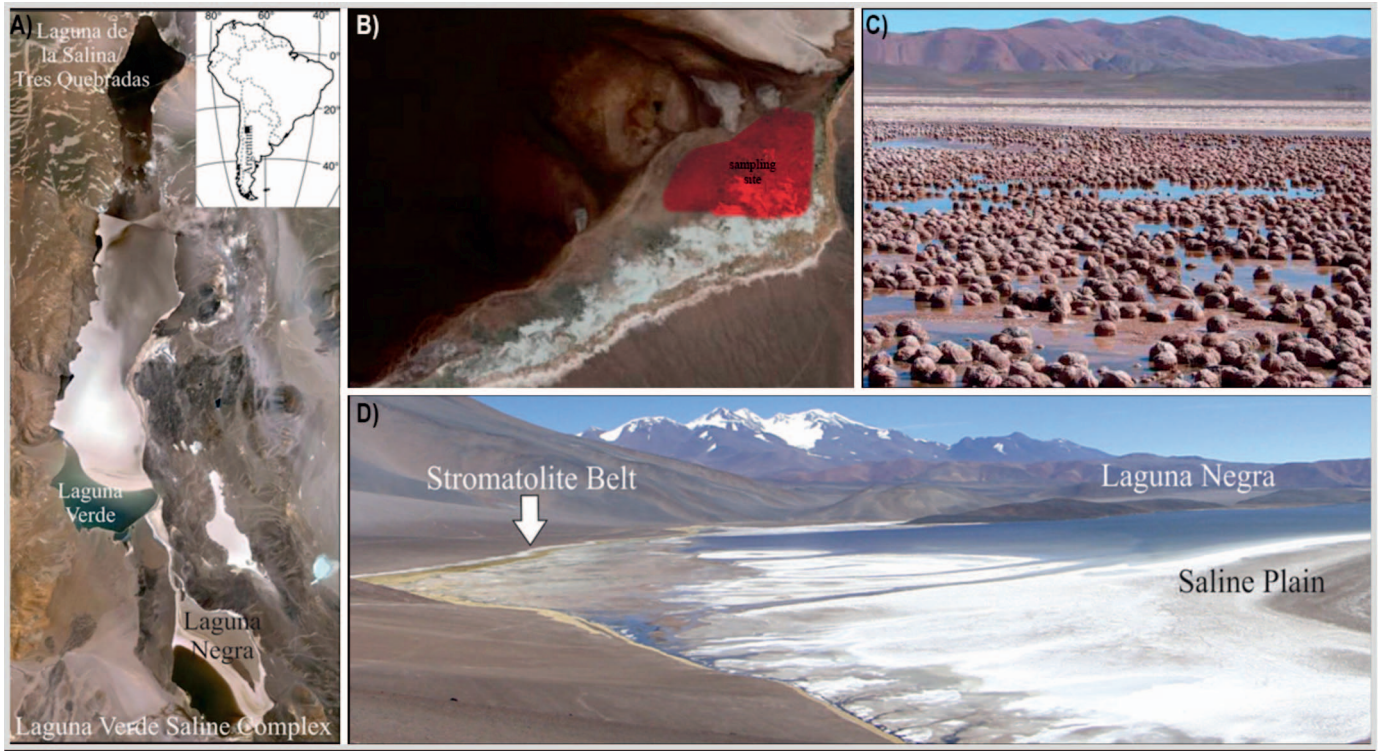

FIG. 1.—**A)** Location map of the Laguna Verde Saline Complex (Catamarca Province, northwest Argentina), including the Laguna Negra at the southern end, which is the focus of this work. **B)** Satellite image with a closer view of the Laguna Negra southern edge showing the sampling site area. **C**, **D)** Panoramic view of the carbonate Stromatolite Belt. Note in Part C the partially exposed decimeter-size microbial carbonates that compose most of it.

1999; Dittrich and Sibler 2010; Kamennaya et al. 2012; Bundeleva et al. 2014), sulfate-reducing bacteria (Vasconcelos et al. 1995; Bosak and Newman 2003, 2005; Meister 2013), sulfide-oxidizing bacteria (Bosak et al. 2007; Bundeleva et al. 2012), methanogens (Kenward et al. 2009) and more recently, iron-reducing bacteria (Zeng and Tice 2014). In contrast, the influence of eukaryotes, such as diatoms and other microalgae, on carbonate precipitation and microbialite formation has received less attention (Winsborough and Golubic 1987; Awramik and Riding 1988; Winsborough 2000). Numerous works have focused on the ability of cyanobacteria and sulfate-reducing bacteria to produce exopolymeric substances (EPSs) and their influence on carbonate nucleation polymorphs (Kawaguchi and Decho 2002), crystal fabrics, and textures (Gonzalez-Muñoz et al. 2000; Chekroun et al. 2004; Bosak and Newman 2005; Braissant et al. 2007). Diatoms are also known to produce copious amounts of EPS (Awramik and Riding 1988; Stal and Défarge 2005; Underwood 2010; Urbani et al. 2012; Brinkmann et al. 2015), and thus diatom EPS-related calcification is also possible. The interaction between prokaryotes and eukaryotes, such as diatoms, has been the focus of recent research (see Amin et al. 2012 for a recent comprehensive review). These interactions between bacteria and diatoms also need to be explored in regard to carbonate precipitation processes.

This study was designed to explore carbonate mineralization in diatom-rich active microbial mats, developed in a groundwater-fed hypersaline lake in the Puna region of Catamarca, Argentina (Fig. 1A). The Puna region has become a reference area for studying modern microbialites, endolithic microbial communities, and microbial-mat systems (Gomez et al. 2014; Farías et al. 2013, 2014; Rasuk et al. 2014, 2015; Rascovan et al. 2015; Fernandez et al. 2016). Previous work (Gomez et al. 2014; Buongiorno 2014) focused on the texture, mineralogy, and stable-isotope chemistry of the subfossil oncoidal and laminar microbialites. This work explores carbonate precipitation in the microbial mats that are associated with these oncoidal microbialites. The term *oncoids* is used as suggested by Gomez et al. (2014), although alternative terms for similar structures are found in the literature (e.g., *pisoids*, cf. Risacher and Eugster 1979; Jones and Renault 1994; *dendroidal oncolites*, cf. Wade and Garcia-Pichel 2003; and *stromatolitic oncoids* cf. Garcia-Pichel et al. 2004). Information on Bacteria and diatom diversity, together with carbonate microtextures and mineralogy, is discussed in order to compare carbonate precipitation in the active microbial mats and the related current and subfossil oncoids. This is the first survey of these previously unexplored diatom-rich microbial mats, which have developed under the unusually extreme environmental conditions in the Laguna Negra. Results here provide insight on the evolution of microbialite textures and fabrics controlled by changes from prokaryote-dominated systems to mixed eukaryotic–prokaryotic systems.

ENVIRONMENTAL SETTING

The Laguna Negra is located at the southeast end of the Laguna Verde Complex (LVC, GPS S27°38′ 49″, W 68° 32′ 43″), in the southernmost Puna region of Catamarca Province, Argentina (Fig. 1A). The Puna is a high-altitude plateau (average altitude 3700 m with peaks $>$ 6000 m) dominated by volcanic and volcaniclastic rocks, represented mostly by andesitic to basaltic volcanic rocks with minor rhyolite, dacite, and ignimbrite. The LVC consists of a series of lakes and salars resulting from rapid Cenozoic uplift (Jordan and Alonso 1987), progressive environmental restriction (Vandervoort et al. 1995), and increased aridity since the last glaciation (Valero-Garcés et al. 2000).

The Laguna Negra is a shallow ($<$ 2 m) hypersaline lake with an area of 8.63 km^2 (Gomez et al. 2014). The Laguna Negra is a $CaCl_2$-rich brine, where the pH of the main lake and the groundwater springs feeding the lake fluctuates between $\sim$ 6 and $\sim$ 7.8 and salinity between $\sim$ 320 and $\sim$ 9 ppt respectively (for more details in water chemistry, see Gomez et al.

FIG. 2.—Different types of microbial mats recognized by visual inspection and sampled for bacterial diversity studies: **A)** stratified mats (sites LN2), greenish mats (site LN9) and **C)** black pustular mats (site LN5). Note in Part A the development of black pustular mats around partially exposed oncoidal microbialites (white arrow). See Table 2 and text for details.

2014). The mixing zone between the main lake and groundwater is oversaturated with respect to calcite and aragonite, and it is the area were most carbonate precipitation takes place (Gomez et al. 2014).

Immature siliciclastic sediment (mostly silt to sand) and evaporites cover most of the present lake area. The salt flat, located at the northwest margin of the Laguna Negra, constitutes more than 50% of the lake basin, isolating it from the rest of the LVC. Strong winds, high temperatures, and a negative hydrological balance combine to trigger abundant evaporite precipitation (halite, polyhalite, and gypsum; Gomez et al. 2014). Carbonates, typically calcite and minor aragonite, are restricted to the southeastern edge of Laguna Negra (Fig. 1B–D) in a broad (0.3 km^2), shallow-water (< 10 cm) margin, referred to as the *Stromatolite Belt*. The carbonate belt consists of *oncoids*, *stromatolites,* and *laminar crusts* (cf. Gomez et al. 2014) and associated microbial mats (Figs. 2, 3) that are morphologically and texturally different. This work focuses only on the oncoidal structures (Table 1) and the associated microbial mats (Figs. 1B, 2, 3; Table 2).

MATERIALS AND METHODS

Collection and Fixation of Samples

Samples consisted of pieces of bulk homogenized microbial mat from each site (Fig. 2A–C, Table 2), collected in sterile 50 ml falcon tubes and stored at –20 °C until further processing within a week. For microscopy analysis, samples consisted of pieces of microbial mat from each site, collected in sterile 50 ml falcon tubes. Samples for SEM and laser confocal microscopy were stored in Eppendorf tubes and kept at 4 °C. At the laboratory, part of the samples was fixed in a Paraformaldehyde solution at 4 percent for 2h at 4 °C, washed in phosphate buffered saline (PBS), and stored in (1/1) ethanol/PBS at –20 °C until use. Subsamples were also fixed with Glutaraldehyde 2 percent at room temperature overnight and washed in PBS. We also conserved microbial-mats samples without fixation at 4 °C.

Petrography and Mineralogy

Mineralogical composition of carbonates in the microbialites and in the microbial mats were identified by X-ray diffraction using a Philips X'PERT PRO diffractometer housed in the Departamento de Cristaloquímica de la Facultad de Ciencias Químicas, Universidad de Córdoba. Petrographic analysis of carbonate microfabrics was carried out at the microscopy Lab at the CICTERRA (Centro de Investigaciones en Ciencias de la Tierra) using standard polarized-light microscopy equipped with epifluorescence (wideband blue and UV) capabilities.

Scanning Electron Microscopy (SEM)

Microbialites and Glutaraldehyde-fixed microbial mats samples were dehydrated in a gradual series of ethanol baths (10–30–50–70 and 100%). SEM analyses were performed in a FE-SEM Carl Zeiss Sigma Electronic Microscopy at the X Ray Analysis Laboratory (LAMARX Universidad Nacional de Córdoba, Argentina); and with a SEM LEO 1450VP Electronic Microscope in the Electronic Microscopy and Microanalysis Laboratory (LABMEM, San Luis, Argentina).

DNA Extraction, PCR Amplification, and 454 Pyrosequencing

To examine bacterial diversity based on 16S rDNA molecular marker, total genomic DNA was extracted from each site sample (three replicates per site) using the commercially available Power Biofilm DNA Extraction Kit (MoBio, Carlsbad, California, USA). In all cases, 0.2 g of homogenized bulk microbial mat was processed following the manufacturer protocol. Quality was checked by PCR amplification of the bacterial 16S rDNA. In this study, we focused on Bacteria diversity. The V4 hypervariable region of the 16S rRNA gene was amplified from total DNA using the 563F and 802R universal primers, reliable for amplifying, suggested by the Ribosomal Database Project at the Michigan State University (RDP; http//:pyro.cme.msu.edu/pyro/help.jsp). The primers contained the Roche 454 sequencing A and B adaptors and a 10 nucleotide multiple identifier (MID). PCR amplification was done on a FastStart High Fidelity PCR system (Roche Applied Science, Mannheim, Germany) following the manufacturer's instructions. Five independent PCRs were performed to reduce bias. Two negative controls with no template were also performed. The PCR conditions were 95°C for 5 min, followed by 30 cycles of 95 °C for 45 s, 57 °C for 45 s, and 72 °C for 60 s, and a final elongation step at 72 °C for 4 min. The five reactions were pooled, purified, and sequenced on a Genome Sequencer FLX (Roche Applied Science) at the INDEAR genome sequencing facility (Argentina) following the amplicon sequencing protocol provided by the manufacturer.

Analysis of Bacterial Diversity

All analyses of the 16S pyrotags were conducted in the Quantitative Insights Into Microbial Ecology (QIIME) software package v1.7.0 (Caporaso et al. 2010). Sequences were clustered into operational taxonomic units (OTUs) with UCLUST at 0.97 similarity, and the most abundant sequence was used as the OTU representative sequence. Filter parameters were set to reject reads that had mean quality score < 25, maximum homopolymer run > 6, number of primer mismatches > 0, and read length < 200 bp or > 1000 bp. Taxonomic classification of the OTU representative sequences against the Greengenes database was done using

FIG. 3.—**A**, **B)** Stratified microbial mats with associated oncoids. The black arrow shows partially exposed oncoids with irregular external surface with small (millimeter-scale) pillars and shrubs. The centimeter-scale oncoid in Part B shows a smoother external surface still covered with the microbial mat. **C**, **E)** Different oncoidal morphologies and textures as seen on polished cross section (Parts C–F). C) Spherical oncoids with alternating dark-colored and whitish irregular lamina. The inset shows details of the irregular lamina with the typical granular texture (black arrow). **D**, **F)** Polished cross sections showing some of the different lamina types as observed macroscopically, including whitish granular laminae, *Rivularia*-bearing laminae, and alternating sparry-micrite laminae. Note in Part E the shrub-like structures common in these oncoids. For details of the microtextures in thin-sections see Figure 4 and a detailed description in Table 1.

the RDP classifier included in QIIME (bootstrap confidence of 80%). OTU tables were subsampled using 100 replicas for each sampling effort at increasing intervals of 100 sequences; alpha diversity indexes were calculated on each subsample of the rarefaction curve and on the complete OTU table (including all sequences) using QIIME. The calculated Alpha diversity metrics included observed species, CHAO1, Shannon, Simpson, Equitability, and Dominance indexes (Table S1, see Supplemental Material). Samples were compared using the principal-coordinate analysis (PCoA, Fig. 1S, see Supplemental Material) implemented in QIIME, where OTU tables were rarefied and weighted and unweighted UniFrac distance matrixes were built for each rarefied table. A jackknifed replicate PCoA plot was obtained from all these matrixes. A total of 940 OTUs (at 0.97 similarity) were recovered from 8395 quality sequences obtained from all mat samples with an average length of 225 bp, and 1678, 3173, 3544 sequences from stratified, black pustular and greenish mats, respectively. The sequences were deposited as FASTAQ in the NCBI Sequence Read Archive (SRA) under the accession number SRP066052.

Imaging by Confocal Laser Scanning Microscopy (CLSM)

Before embedding, millimeter-size pieces of formaldehyde-fixed microbialites with associated biofilm were stained with DAPI at 1 mg/ml for 2 h at room temperature and calcein, at 0.1 mg/ml, at 4 °C during 48 h (Gerard et al. 2013). After staining, microbialite fragments were dehydrated in a gradual series of ethanol baths (30%, 50%, 70%, 90%, and 100%), and progressively impregnated with hard-grade LR-white resin (Polysciences,

TABLE 1.—*Carbonate microbialite lamina textures and microfabric (see Fig. 4 for details).*

Microbialite Type	Microfabric Elements	Observations
Oncoids: cm- to dm-scale concentrically laminated discs, spheres and flattened domes	Alternating micritic and botryoidal laminae (cf. Gomez et al. 2014).	Mostly developed in ponds with the pinkish to orange stratified mats (Figs. 2A, 3A, B). Alternating micritic and botroidal lamina are usually irregular with variable thickness (50–500 μm thick, Figure 4A–C). These are the most common lamina types in these structures. *Micritic*: represented by nanometer-scale spherical, globular, or spherulitic calcite (up to 300 nm) or more irregular globular to anhedral calcite. *Botryoidal*: Individual or stacked micro-laminated botryoids (300 m wide and 100 m tall) or radial-fibrous crystal bundles (50–100 μm wide 400–600 μm tall) associated with bacteria remains and diatom frustules.
	Locally microspar lamina with preserved *Rivularia*-like filaments	Laminae bearing *Rivularia*-like filaments: Irregular laminae with tufted dark brown to yellowish vertically oriented filaments (diameter 15–20 μm) in micro-spar translucent carbonates (Fig. 4D–F). Filaments form a paintbrush-like (cf. Reitner et al 1996) palisade fabric. Alternates with micrite or botryoidal laminae.
	Whitish irregular granular laminae	White granular precipitates with presence of diatom and forming irregular laminae alternating with other lamina types (Fig. 4D–F, J–K). It shows characteristic remarkably similar to the granular texture and diatom–bacteria aggregates observed in the stratified pinkish-orange microbial mats thus being an fossilized equivalent.
	Spar to microspar laminae with oriented pennate diatoms	Irregular and translucent microspar laminae, occasionally micritic. Parallel-oriented pennate diatom frustules (Fig. 6). This has also been recorded during diatom blooming events in the areas where the pinkish-orange microbial mats are common (Fig. 6).

Inc.). The samples were incubated for 18 h at 4 °C in a (1/1) then (2/1) mixture of LR-white/ethanol and finally in pure LR-white resin. After 2 h at room temperature, samples were embedded in pure LR-white resin for 1 h at 40 °C and then for 24 h at 60 °C. After polymerization, transverse sections were cut with a diamond wire and polished (diamond powder 0.24 μm) to a final thickness of about 50 μm.

Samples without embedding were stained with SytoR9 (green fluorescent nucleic acid stains) at a concentration of 10 μM (Invitrogen) for 1 min, then washed for a few seconds in cold water and left to dry; finally covered by Citifluor AF3 (glycerolmountant solution from Emgrid) (see details in Gerard et al. 2013).

RESULTS

Three main types of microbial mats (Fig. 2, Table 2) are visually recognized, and these were characterized by Bacteria 16S rDNA analysis: 1) *stratified pinkish to orange mats* (Fig. 2A) (LN2), 2) *greenish mats* that occasionally show convex-upward horizons given by cohesive mats floating on gas bubbles (site LN9) (Fig. 2B), and 3) *black pustular mats* (site LN5, Fig. 2A, C). The well-stratified pinkish to orange microbial mats are associated with oncoids (Fig. 2A). The soft greenish mats are typically located at groundwater springs, where oncoids are present though less frequent (Fig. 2B). The black pustular mats locally encrust partially exposed oncoids (Fig. 2A) or form discontinuous patches, covering the partially exposed carbonate substrate (Fig. 2C).

Oncoids: Morphology, Textures, and Mineralogy

Previous work (Gomez et al. 2014) has shown that oncoids represent the bulk of the stromatolite belt (Fig. 1C) and consist of centimeter to decimeter-scale (up to ∼ 35 cm diameter) spheres, discs, and flattened domes (Fig. 3A–E). These oncoids can have smooth external surfaces (Fig. 3B), different kinds of external lateral ridged protrusions, and more complex millimeter-scale pillars and shrub-like protrusions (Fig. 3D, E; see also Gomez et al. 2014). These oncoids can be observed as decimeter-size subaerially exposed and hardly cemented, or smaller subaqueous oncoids (but morphologically and texturally similar) associated with different kinds of microbial mats as described in Table 2 (Figs. 2, 3A, B).

TABLE 2.—*Microbial mat types and sample location (see Fig. 2).*

Mat Type	Site	Observations	Sample Location (GPS)
Stratified	LN2	Well-stratified pink to orange mats, showing discrete layers and usually located within ponds 3–10 cm deep and associated with oncoids (Fig. 2A–C) where salinity reaches 120 ppt (cf. Gomez et al. 2014). The upper layer (Layer I) can be pink to orange as well as yellowish-golden coloured, usually has 1–2 cm thick and the mid-purple layer (Layer II) typically reaches 2–5 mm thick. The black anoxic horizon (Layer III) can be several cm to dm thick. See Figures 2A and 5.	S 27°38′45.6″ W 68°32′37.44″
Greenish	LN9	Greenish soft bubble floating mats: typically located at groundwater springs, where salinity is lower (16 ppt, cf. Gomez et al. 2014). See Figures 2B and 7.	S 27°38′52.6″ W 68°32′38.7"
Black Pustular	LN5	Dark gray to black pinnacle to pustular mats (Figs. 2C, 8). Usually located close to the water–air interface, partially exposed as patches covering carbonate crusts (Fig. 2C) or as peripheral rims around oncoids (Fig. 2A).	S 27°38′45.6″ W 68°32′37.44″

When observed in cross-section, oncoids are broadly concentrically laminated (Fig. 3C), although some asymmetrical growth is also seen (Fig. 3D, E). Lamination is composed of different laminae types (see Table 1) and mostly represented by alternating irregular whitish, greenish, to black or red laminae (Fig. 3D–F; see more details about laminae types in Table 1), given by variable organic and trace-element contents (Buongiorno 2014). Under the transmitted-light microscope, these laminae are typically characterized by irregular hybrid micro-textures, usually composed of alternating irregular micritic and botryoidal laminae, although other laminae types are also present (see Table 1, Figs. 3F, 4A–C; Gomez et al. 2014 and this work). Regarding mineralogy, both aragonite and calcite can be present in all fabric types, although in oncoids aragonite laminae is always subordinated when compared to calcite (Gomez et al. 2014; Buongiorno 2014).

As mentioned, in addition to sparry botryoidal and micrite laminae (previously described in Gomez et al. 2014), in the oncoids other lamina types were here recognized (see details in Table 1). When the oncoids are partially exposed these can be colonized and encrusted by the black pustular mats composed by filamentous (*Rivularia*-like) Cyanobacteria, which usually are located close to the air–water interface (Fig. 2A). This is also observed inside the oncoids as brownish irregular laminae with tufted vertically oriented filaments represented by *Rivularia*-like cyanobacteria filaments forming a palisade fabric and these alternate with other lamina types (Figs. 3E, 4D, F, Table 1). Within the oncoids, in addition to the *Rivularia*-bearing laminae, diatom-rich laminae are common. These are recorded as micrite to microspar-rich whitish, irregular granular laminae of variable thickness (Fig. 3D, E, and details in Table 1). These laminae show abundant diatoms occasionally visible as part of subspherical aggregates (Fig. 4E, G). In addition, sparry laminae with parallel-oriented pennate diatoms are recorded and alternating with other laminae types (Fig. 4H, I, Table 1). Under CLSM some pigments and diatom remains are also still observed in these aggregates (Fig. 4J, K).

Microbial Mats, Diatoms and Associated Carbonates

The three-group microbial-mat division (stratified, greenish, and black pustular mats), first based on the macroscopic aspect of the mats (Table 2), is confirmed by unweighted and weighted UniFrac PCoA analysis (Fig. 1S). Differences in the mat structure are also observed in the bacteria diversity between the stratified, the greenish, and the black pustular microbial mats.

A common feature observed throughout the Laguna Negra mats is the abundant presence of subspherical aggregates composed of diatoms and filamentous and coccoid Cyanobacteria, together with other microbial groups. These diatoms and prokaryotic cells are usually embedded in exopolymeric substances (EPS), where abundant carbonate precipitation takes place (Figs. 5–8). The complex bacterial community observed by CLSM was also confirmed during the Bacteria diversity analysis by 16S pyrotags. As is shown here, carbonates (typically calcite) are spatially associated with exopolymeric substances. These aggregates were present in all mat types (Figs. 5, 7, 8), and in the black pustular mats, where they appear to be trapped between Cyanobacteria filaments (Fig. 8). In contrast, abundant aragonite was locally observed during diatom-bloom events (see details in next section, Table 3 and Fig. 6).

Stratified Mats

Stratified mats are typically subaqueous (usually in ponds 3 to 10 cm deep), and associated with decimeter-scale spheroidal oncoids (Fig. 2A, Table 3). These mats show the typical stratified internal structure (Fig. 5A) commonly seen in microbial mats in hypersaline settings (cf. Teske and Stahl 2002). Layering is recognized by different-colored zones as observed in cross-section: Layer I is typically pink to orange as well as occasionally yellowish-golden (up to 2 cm thick), Layer II is purple and thin, typically 2–5 mm thick, and Layer III is thicker (several centimeters to decimeters thick) and black (Fig. 5A).

Scanning Electron Microscopy (SEM).—When observed under SEM these mats show abundant carbonate precipitation associated with the diatom–bacteria aggregates (Fig. 5B–E). Mineral-entombed diatom aggregates are visible throughout the mat (through Layer I to III). The diatom–bacteria aggregates are subspherical in shape and typically range between 50 and 200 μm in size (Fig. 5B, C). Some diatoms are occasionally located at the outer region of the aggregates (Fig. 5C), and some diatom frustules have also been observed protruding from the EPS matrix (Fig. 5F). Diatoms are usually preserved, with no clear evidence of fragmentation or corrosion. Filamentous structures are also present (Fig. 5B), mostly cyanobacteria as observed in the CSLM (Fig. 5F).

SEM-EDS and XRD analyses show that carbonates in the aggregates are typically represented by anhedral, nanometer size globular to spherical (spherulite-like) calcite particles (Table 3, Fig. 5B–E). These particles are usually less than 0.5–1 μm in diameter and are located inside the EPS matrix (Fig. 5B). These can be represented by isolated individuals inside the EPS matrix, or as small clusters that coalesce to form bigger aggregates. More irregular grumulouse textures with smaller crystals inside the EPS are also recorded. Although subordinated, subhedral to euhedral particles are locally present.

Bacteria and Diatom Diversity.—Within Bacteria *Bacteroidetes* (22%) was the dominant phylum, and the dominant family detected was *Rhodothermaceae* (14%). *Proteobacteria* was found second in abundance (19%), and most of it belonged to the *Desulfobacteraceae* family (10%) in the δ-proteobacteria class. The phylum *Spirochaetes* was also present (14%). *Deinococcus-Thermus* (8%) and *Firmicutes* (4%) were less abundant (Fig. 9). Representative cultivated species belonging to the *Rhodothermaceae*, *Spirochaetaceae*, and *Deinococcaceae* families are mostly heterotrophic saccharolytic bacteria (Makarova et al. 2007; Karami et al. 2014; Park et al. 2014). Whereas cultivated representative members of the *Desulfobacteraceae* family are generally heterotrophic sulfate-reducing bacteria, autotrophic representative species also exist.

The diatoms recognized by light microscopy and SEM analysis in the stratified microbial mat are *Achnanthes brevipes* sp., *Halamphora* sp., *Denticula* sp., *Haloroundia Speciosa* sp., *Nitzschia* sp., *Navicula* sp., *Surirella* sp., and *Striatula* sp.

Confocal Laser Scanning Microscopy (CLSM).—Abundant diatoms are observed by CLSM in Layer I. Although not detected by pyrosequencing, some ovoid and filamentous cyanobacteria were also observed (Fig. 5F–H). Mineral aggregates (light blue to grayish) (Fig. 5G, H) with entombed diatoms are visible. In the deeper part of this layer, abundant non-photosynthetic microorganisms (in accordance with the pyrosequencing data) were detected by Syto9 DNA staining (green) and are associated with calcite mineral grains (Fig. 5H). The second layer (Layer II) is a purple thin horizon whose coloration is related to the presence of purple sulfur bacteria (PSB). CLSM observations highlight a conspicuous amount of PSB, which were also detected in the pyrotag data. These belonged to the *Chromatiales* order, which are anoxygenic photosynthetic bacteria that use hydrogen sulfide as electron donors and accumulate elemental sulfur in globules inside their cells (Imhoff 2015). The globules were detected by laser reflection under CLSM (bright blue in Fig. 5G) and confirmed as sulfur by SEM-EDS. CLSM observations show that PSB were entombed in calcite aggregates together with diatom remains (Fig. 5G). Layer III is thick, anoxic, and black. Numerous rod-shaped and cocci microorganisms, as well as rare filamentous non-photosynthetic microorganisms were detected in this layer (Fig. 5H). Mineral-entombed diatoms and Cyanobacteria were still detectable because

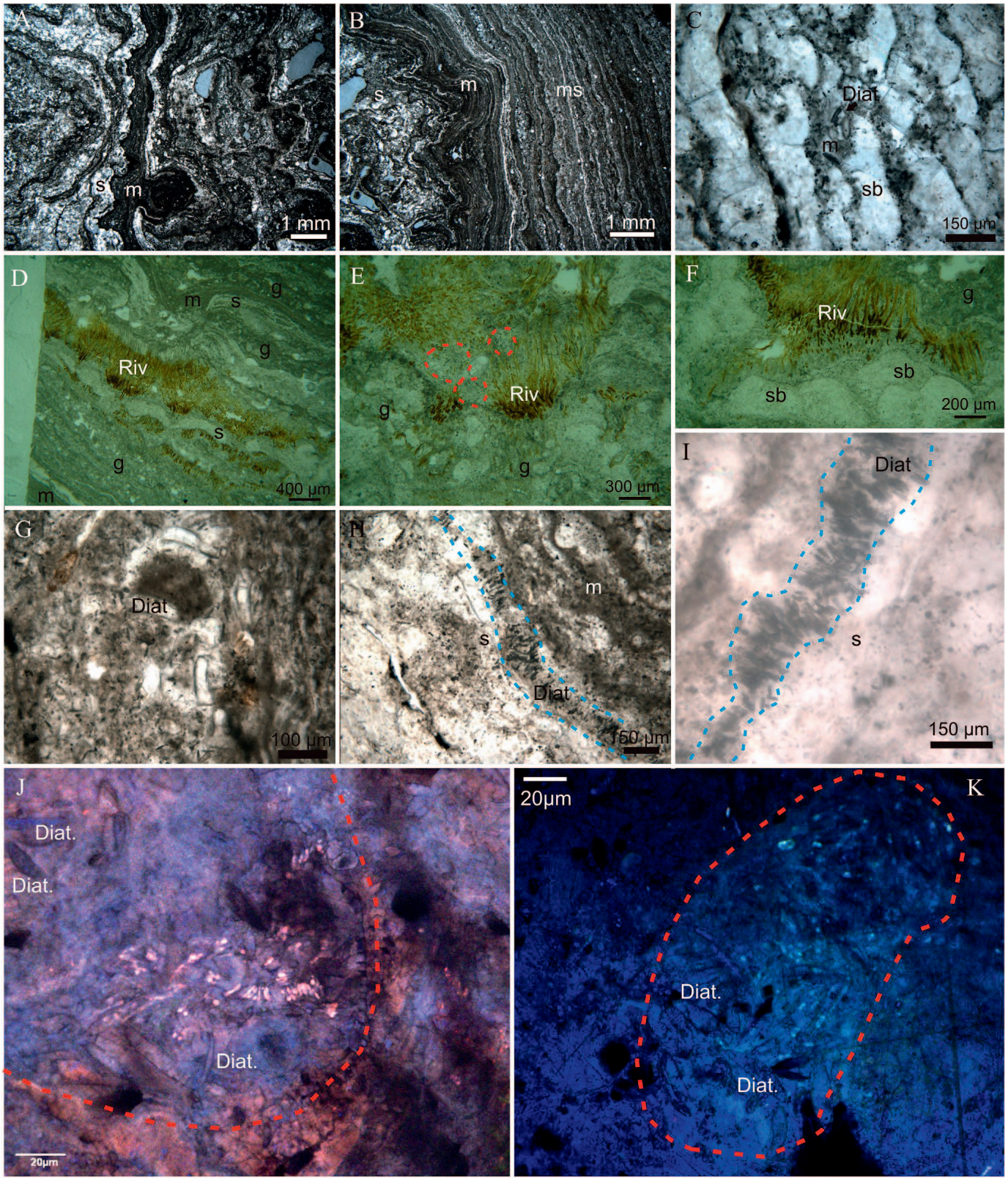

FIG. 4.—Light microscopy (A–I) and CSLM (J–K) images of the diversity of carbonate microtextures as observed in the Laguna Negra oncoids (for more details see also main text and Table 1). **A)** Irregular alternation of sparry (s) and wrinkled micritic (m) laminae. **B)** Transition from irregular sparry (s) and micritic laminae (m) (left) to more regular thinly laminated and predominatly micrite-sparry laminae (right) (ms). **C)** Translucent sparry laminae composed ofstacked botryoids (sb) alternating with darker micritic to microspar (m) laminae with organic remains including diatom frustules. **D**, **E)** Diversity of textures recorded in oncoids and as observed by light microscopy including: micritic (m), sparry (s), diatom-rich granular (g) laminae alternating with filamentous-rich laminae represented by entombed cyanobacteria (*Rivularia*-like, Riv.)

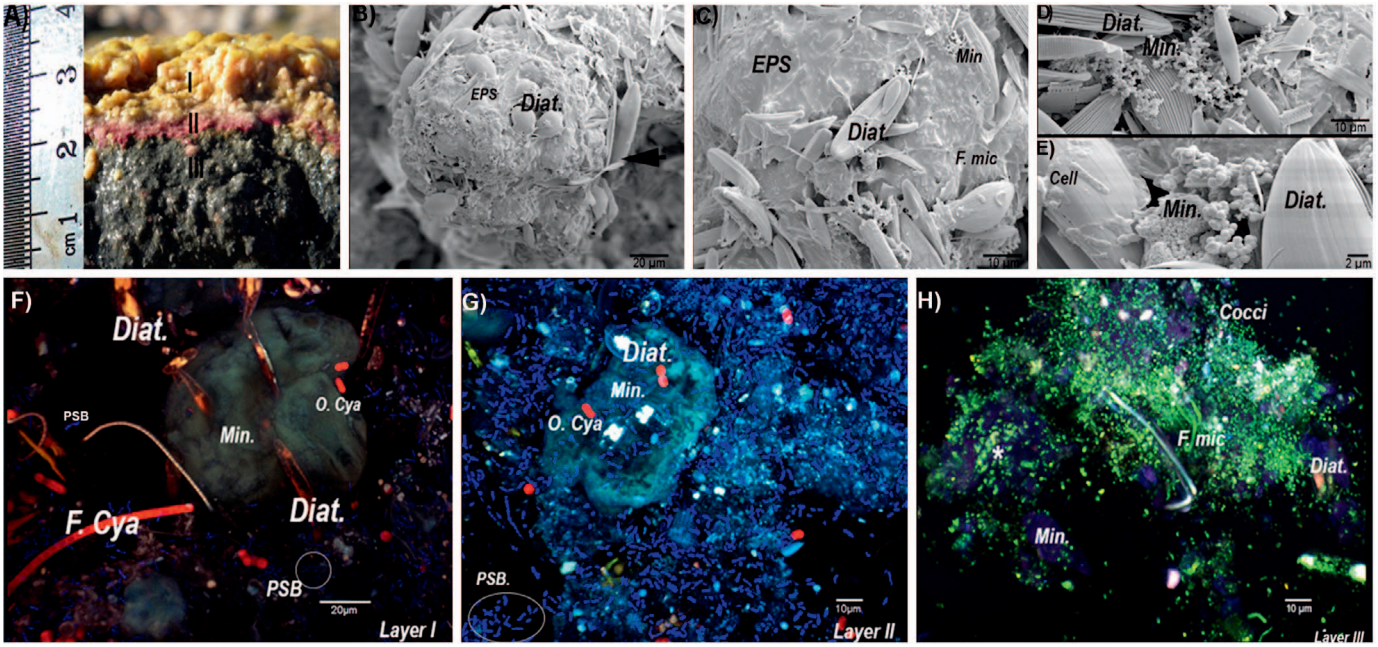

FIG. 5.—Field (Part A), scanning electron microscopy (SEM, Parts B–E) and confocal laser scanning microscopy (CLSM, Parts F–H) images of microorganisms associated with the well-stratified mat (LN2 site) in the Laguna Negra. **A)** Characteristic stratified mat, Layer I: yellowish-gold upper layer; Layer II: purple middle layer, and Layer III: black lower layer. **B)** SEM image of a subspherical aggregate (black arrow) surrounded by EPS and diatoms frustules. **C)** High-magnification image of an aggregate where EPS and diatoms frustules are more visible, as well as filamentous microorganisms (F. mic) and calcite grains (Min) (confirmed by CLSM and XRD respectively). **D**, **E)** SEM images showing a closer view of nanoglobular to spherulitic carbonates (Parts D, E, Min); arising between diatom frustules and EPS. Some microbial rod-shaped cells are also observed. F–H) Composite three-colors CLSM images of microorganisms from Layer I to III obtained with a concomitant excitation at wavelengths of 405 nm, 488 nm, and 633 nm. **F)** Autofluorescent photosynthetic microorganisms in Layer I (bright red and yellow color). Abundant diatoms (Diat), some ovoid (O. Cya) and filamentous cyanobacteria (F. Cya) and few purple sulfur bacteria (PSB) are visible. PSB are anoxygenic photosynthetic bacteria oxidizing hydrogen sulfide. They are observable thanks to the reflection of the blue laser (405 nm) on the elemental-sulfur globules accumulated in their cells and appearing in deep blue (white circle). Mineral grains (Min), calcite as suggested by XRD and SEM data, with entombed diatoms and PSB clearly visible. **G)** In Layer II fewer diatoms (Diat) are observed, but the calcite grains with entombed diatoms are still observable in a conspicuous amount of PSB. **H)** In Layer III, abundant mineral grains (Min) are detectable in light blue. Few diatoms (Diat) are visible, and most of them are encrusted in the mineral where photosynthetic pigments are still detectable. The overwhelming majority of the microorganisms are detectable only thanks to Syto 9 staining (green fluorescence). Cocci and filamentous microorganisms appear closely associated with minerals.

of their photosynthetic pigments (Fig. 5H). Rod-shaped microorganisms were also observed inside the frustules of some diatoms.

Blooms of Pennate Diatoms Associated with the Stratified Mats.— In the microbial ponds where the stratified mats are common, occurrences of *whiting*-like (cf. Thompson et al. 1997) precipitation have been observed locally where carbonate precipitation is taking place. These usually are suspended a few centimeters above the sediment–water interface and overlying the microbial mats (Fig. 6A). Remarkably, these correspond to pennate-diatom (*Nitzschia* genus of around 30–40 µm long, 5–8 µm wide) blooming events, where diatom frustules are parallel to each other. Abundant precipitation of aragonite and calcite takes place, as detected by XRD (Fig. 6B–D), producing a milky-white-color precipitate, which is deposited over the microbial mats (Fig. 6A). Aragonite is represented by euhedral to subhedral crystals, usually by needles that are up to 2 µm long and less than 0.2 µm wide (Fig. 6C, D). No EPS was observed related to these aragonite-rich precipitates. More irregularly shaped euhedral to subhedral calcite crystals are also present (Fig. 6D). The carbonates related to these pennate diatom blooms are mineralogically and texturally different when compared with the carbonates typically found inside the microbial mats and associated with the EPS matrix, since when EPS are present these are represented by nanometer-size anhedral subspherical to globular calcite particles (see details in Table 3).

Greenish Mats

The greenish mats are not stratified, show a bright greenish color, and occasionally show convex-upward horizons given by cohesive mats floating on gas bubbles (Figs. 2B, 7A). Oncoids are present, although they are less frequent when compared with the stratified mats. These oncoids are of centimeter-scale and more flattened than spherical. Greenish mats are commonly located at groundwater springs where salinity is low (16 ppt; cf. Gomez et al. 2014).

Scanning Electron Microscopy (SEM).—The diatom–microbe aggregates are subspherical to slightly elongated, and are usually 40–100 µm in

←

filaments. Note in Parts D and E the subspherical diatom-rich aggregates (some of them highlighted in red, **E)** that are common in the granular diatom-rich lamina and represent entombed diatom–bacteria aggregates. **F)** Detail of *Rivularia*-like filaments encrusted on sparry laminae represented by translucent stacked botroidal crystals (sb). **G)** Close view of a diatom-rich micritic to microsparitic laminae (Diat) with darker organic remains. **H**, **I)** A lamina with oriented pennate diatoms (blue dotted line) alternating with other laminae types (m and s). **J**, **K)** CSLM images of laminae underlying the black pustular (*Rivularia*-like) microbial mat where diatom–bacteria aggregates (highlighted in red) can be observed. Note the abundance of diatoms frustules (Diat.) and photosynthetic pigments highligthed by pigment fluorescence under the confocal microscope.

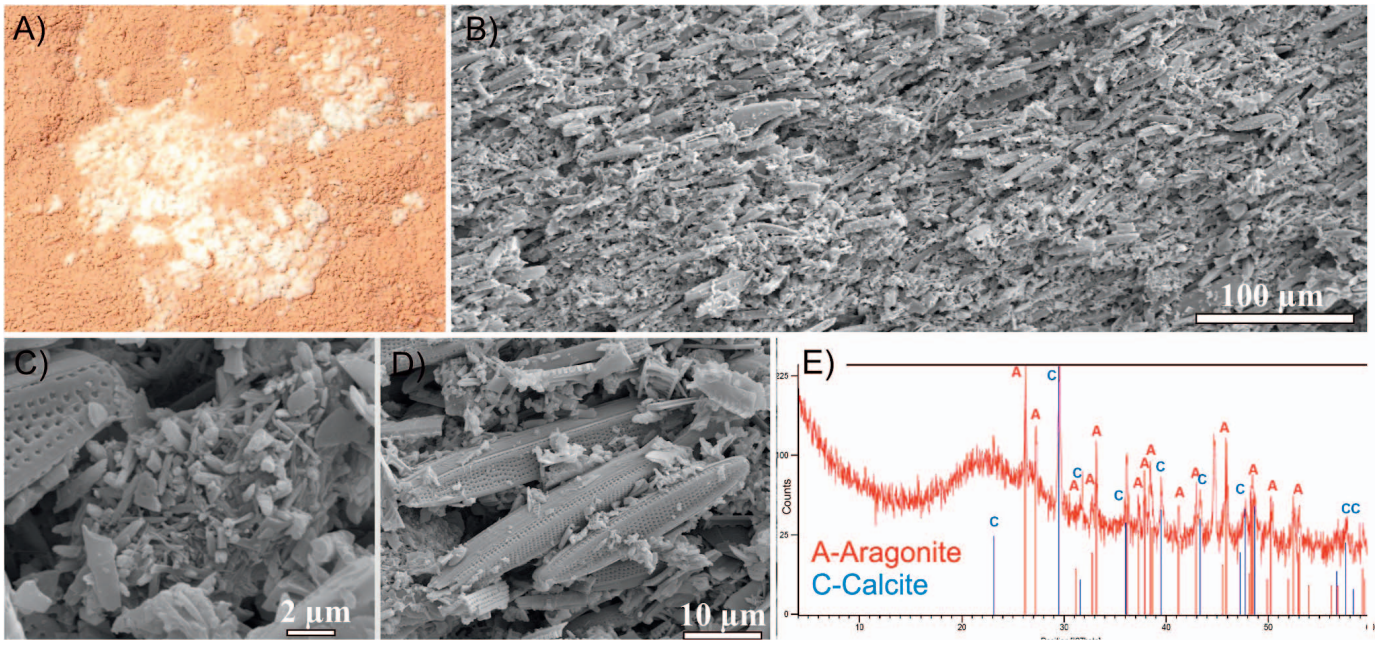

FIG. 6.—**A)** Pennate-diatom blooming events with aragonite precipitation (white-colored material) developed overlying the stratified pink to orange microbial mats. The horizontal field view of the picture is about 30 cm wide. **B)** SEM image of the white-colored precipitated material with pennate diatoms oriented parallel to each other. **C**, **D)** SEM images of needle-shaped euhedral aragonite crystals and associated diatoms. **E)** XRD diagram showing aragonite (A) plus calcite (C) peaks.

diameter (Fig. 7B). Diatoms can be observed inside the aggregates, as well as at the outer edge. They are usually well preserved, and significant fragmentation or corrosion features of frustules are rare (Fig. 7B, C). Filamentous, coccoid and rod-shaped bacteria are also observed. Carbonates, similar to other aggregates, are represented by calcite and are mostly subspherical to nano-globular aggregates up to 500 nanometers in size. They are found as isolated particles or forming bigger clusters in the EPS matrix (Fig. 7C). More irregular and smaller-size subhedral carbonate particles are also present, although subordinate.

Bacteria and Diatom Diversity.—The most abundant bacteria detected by pyrosequencing belonged to the *Bacteroidetes* phylum (30%). Roughly 17% of them corresponded to the *Saprospiraceae* family, which is known to have an important role in the breakdown of complex organic compounds (McIlroy and Nielsen 2014) (Fig. 9, and Figs. S1 and S2, see Supplemental Material). Meanwhile, 11% belonged to *Flavobacteriaceae* family. *Verrucomicrobia* phylum was abundant as well, with a representation of 26%. *Proteobacteria* phylum were found in 18%, and α-proteobacteria represents the 83% of the relative abundance in this group. Most of it belonged to *Rhodobacteraceae* family. Compared with all the other mats, the phylum *Deinococcus–Thermus* was not represented in this mat (Fig. 9). In the greenish mats the classified diatoms include *Achnanthes brevipes* sp., *Mastogloia* sp., *Diploneis* sp., *Halamphora* sp., *Navicula* sp., *Surirella striatula*, and *Campilodiscus* sp.

Confocal Laser Scanning Microscopy (CLSM).—The transition from the active precipitating parts of the mats to the deeper fossilized parts was observed in epoxy-resin-embedded samples. The diatom–bacteria aggregates previously described in the SEM section were also recognized under CLSM (Fig. 7D, E). Diatoms are observed due to their photosynthetic pigments and some bacteria due to DAPI staining (Fig. 7D). The aggregates show a core with carbonates (calcite) and entombed diatoms (still visible by partially degraded pigments) and an outer edge with active diatoms. Free Ca^{2+} is recognized under CSLM by calcein staining (Fig. 7D, E). As observed in Figure 7E, diatoms and bacteria became progressively entombed in calcite. The progressive entombment (from left to right in Fig. 7E) of the mat cements or fuses the micro-calcite aggregates together, forming more continuous laminae (right side of Fig. 7E).

Black Pustular Mats

These mats show a black pustular surface and are in areas where the substrate (e.g., oncoids or sediments) is exposed and grow close to the air–water interface or partially exposed (Fig. 2A) where desiccation and UV radiation influx are important. They are observed locally encrusting the rims of partially exposed oncoids or forming discontinuous patches, covering the partially exposed carbonate substrate (Fig. 2C).

Scanning Electron Microscopy (SEM)

Diatom–bacteria aggregates are subordinate but present in the black pustular mats, and they appear attached to or trapped between Cyanobacteria filaments (Fig. 8A–C). Aggregates are subspherical to more irregularly shaped (Fig. 8B), typically $<$ 100 µm in diameter and with abundant diatoms, filaments, and coccoid and rod shaped bacteria within an EPS matrix. The observed carbonates within the aggregates are anhedral, nanometer size (250 nm) globular to spherical particles (Table 3, Fig. 8B, C). Irregular grumulouse clusters of carbonate particles are also common. The carbonate minerals, as in other aggregates are represented by calcite.

Bacteria and Diatom Diversity.—The black pustular mat presented the highest dominance index and the lowest equitability (Table S1, see Supplemental Material). *Deinococcus–Thermus* (*Deinococcaceae* family 37%), *Verrucomicrobia* (17%) (*Spartobacteriaceae* family 10% and *Puniceicoccaceae* family 4%), *Cyanobacteria* (11%), and Proteobacteria (10%) (Fig. 9 and Fig. S2) are the most abundant phylum. With the

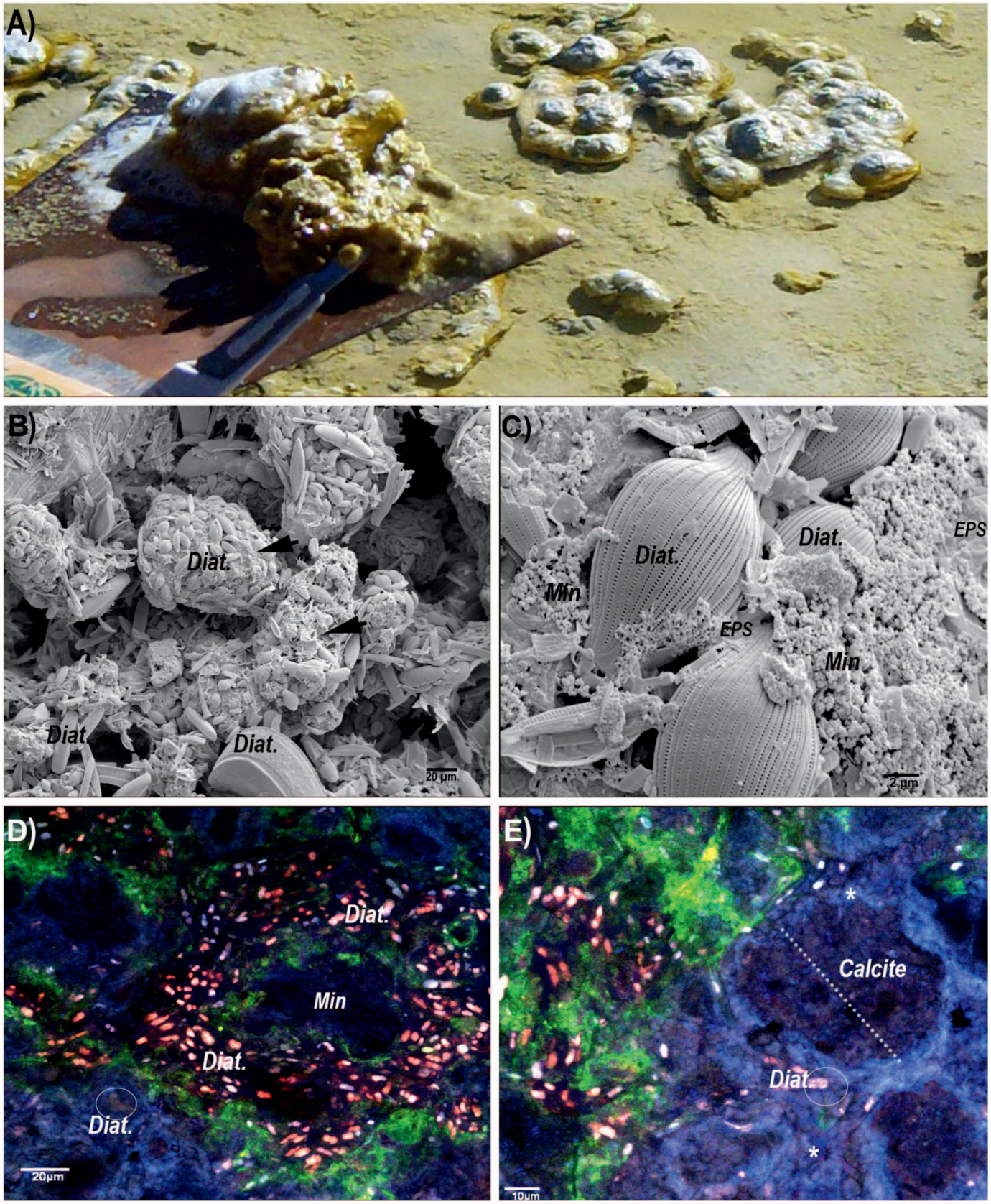

FIG. 7.—Field, (Part A), SEM (Parts B–C) and CLSM (Parts D–E) images of microorganisms associated with the greenish mat. **A)** The greenish mat shows soft, more cohesive pieces floating on gas bubbles on the surface of the mat. **B)** SEM image of several subspherical aggregates (black arrows) covered with diatoms. **C)** Closer view of

exception of Cyanobacteria, most of the bacteria were heterotrophic. All the cultivated members of the most abundant family detected, *Deinococcaceae*, are saccharolytic (Makarova et al. 2007).

The recorded cyanobacteria show morphology, habit, pigmentation and heterocyst presence similar to *Rivularia* sp. The 16S rDNA most abundant Cyanobacteria pyrotag shows 96.89% identity with *Rivularia* atra BIR MGR1 (GenBank Accession Number AM230675.1). Filaments were between 10 and 15 μm in diameter; the dark brownish-yellowish color (Fig. 8A) is probably related to the presence of pigments such as scytonemin (Garcia-Pichel and Castenholz 1994; Rastogi and Incharoensakdi 2014). In the black pustular mats the diatoms were *Haloroundia speciosa* sp., *Denticula* sp., *Brachisira* sp., *Navicula* sp., *Diploneis* sp., and *Surilella* sp.

Confocal Laser Scanning Microscopy.—Confocal-microscopy images confirmed the presence of a microbial community inside the aggregates that are associated with the *Rivularia* filaments (Fig. 8E, F). At the surface and inside the microorganism–mineral aggregates diatoms were clearly detected by CLSM (Fig. 8E). Calcite-mineral precipitates are associated with pigmented cocci cells, diatoms, and EPS (Fig. 8D, F). These irregular to globular mineral grains become bigger and more abundant closer to the *Rivularia*-like filament that lead to the progressive entombment of the filaments (Fig. 8E). Thus, calcite precipitation together with free Ca^{2+} ions (visible in green by calcein staining) are observed on the EPS around *Rivularia*, but not specifically on the *Rivularia* sheaths (Fig. 8E, F).

DISCUSSION

Carbonate Textures in Microbial Mats and Oncoids

Some lamina patterns and textures recorded inside the subfossil oncoids (Fig. 4, see detailed fabric descriptions in Table 1) are comparable with those observed within the microbial mats, suggesting comparable processes (Tables 1, 3). For example, when submerged, the oncoids were observed in ponds with the pink stratified mats which are precipitating a set of carbonate textures including micritic diatom–bacteria carbonate aggregates (Fig. 4E, G, J, K, Tables 1, 3). These are preserved inside the oncoids as irregular whitish granular diatom-rich textures and as a key component in the laminated structure. In addition these alternate with other lamina types like irregular micrite and botryoidal sparry laminae (Fig. 4C–F) that have been interpreted as produced with variable degrees of microbial influence (Gomez et al. 2014). In contrast, when oncoids are partially exposed, they are colonized by the black pustular mats (Fig. 2A), which are then preserved inside the oncoids as discontinuous laminae with filamentous tufted, paintbrush-like palisade fabrics (Fig. 4D, F, Table 1).

Pennate-diatom blooming events occur, probably induced by local environmental changes. These blooming events trigger carbonate precipitation represented by aragonite needles with oriented pennate diatoms (Fig. 6A–D). This is also recorded inside the oncoid as discontinuous laminae with oriented pennate diatom-rich laminae that alternate with the other lamina types (Fig. 4H, I), showing that these also contribute to oncoids lamina accretion. These observations suggest that subtle lake-level and environmental fluctuations in the ponds have some control on the type of microbial mat and thus the related carbonate textures. Such environmental indicators are recorded as different alternating lamina types inside the oncoids (Fig. 4, Table 1).

Diatom–Bacteria Aggregates Formation

Our work in the Laguna Negra has shown the presence of diatom–bacteria aggregates where abundant carbonate precipitation takes place. The reasons and mechanisms of diatom–bacteria aggregation are not clear and are beyond the scope of this work, but some considerations can be made.

Aggregation of diatoms in marine systems is commonly observed after oceanic diatom blooming events (Riebesell 1991; Buck and Chavez 1994). Diatoms are known to produce significant amounts of exopolymeric substances (Bellinger et al. 2005; Stal and Défarge 2005) that bacteria can oxidize for a source of nutrients and energy (Waksman et al. 1937; Murray et al. 1986).

Environmental conditions in Laguna Negra can be particularly important to understand the diatom–bacteria aggregates and diatom–bacteria interactions in this system. Aggregation of diatoms and bacteria has been suggested to occur by charge neutralization with Ca^{2+} ions (by binding of calcium to negatively charged teichoic acid) on both the bacteria and diatom cell surfaces (Powell and Hill 2014). In addition, cations like Ca^{2+} and Mg^{2+} affect EPS structure and its rheological properties (Thornton 2002), and Ca^{2+} is important for fouling diatom adhesion to negatively charged surfaces (Cooksey 1981). Laguna Negra is composed of a $CaCl_2$ brine (Gomez et al. 2014); thus Ca^{2+} is particularly abundant. This, along with the abundant production of negatively charged EPS by both diatoms and bacteria, could potentially influence aggregation. Given their abundance, diatoms may play a main role in EPS production (cf. Bellinger et al. 2005; Stal and Défarge 2005) in the Laguna Negra microbial mats and thus formation of aggregates.

Diatom–bacteria aggregates have been reported (biomicrospheres, cf. Brehm et al. 2004, 2006). In this case, through a symbiotic relationship between diatoms, cyanobacteria, and heterotrophic bacteria, these aggregates were able to induce calcium carbonate precipitation (Brehm et al. 2004, 2006). Brehm (2004) mentioned that aggregation of biomicrospheres can be an advantage, for example as protection from grazing, improved transport in the water column, and better access to light and/or nutrients (cf. Brehm et al. 2004, 2006). *In vitro* culturing has shown that carbonates do not precipitate in the absence of microorganisms (Brehm et al. 2004). Our work in the Laguna Negra highlights the importance of EPS production by diatoms as well as the role of the microbial component in carbonate precipitation within aggregates, and this is also supported by previous work (Brehm et al. 2004, 2006).

EPS Related Calcium Carbonate Precipitation and Bacteria Diversity

The carbonate particles that precipitated in the EPS matrix inside the Laguna Negra aggregates share common characteristics (location, size, morphology, microtexture and mineralogy) regardless of the different mat types (Figs. 4, 5–8 and see Table 3 for details). They do show remarkable differences when compared with those developed without EPS influence (Fig. 6C, D), as it is the case of carbonate precipitation related to diatom blooming events (Figs. 6, Tables 1, 3), suggesting different controls.

Carbonate Precipitation Associated with EPS

Diatoms and bacteria are known to produce significant amounts of EPS, mostly polysaccharides (Hoagland et al. 1993; Chekroun et al. 2004; Stal

←

one aggregate where diatoms (Diat.), EPS, and calcite (nano-globular aggregates, Min) were observed. **D)** Resin embedded microbialite sample stained with calcein (green fluorescent calcium stain), and DAPI (blue fluorescent DNA stain) with a concomitant excitation at wavelengths of 405 nm, 488 nm, and 543 nm. A high amount of diatoms (Diat.) are visible in the biofilm due to their photosynthetic pigments (red to pink coloration), free Ca^{2+} (green due to calcein stain) is detectable between the active diatoms and the calcite grains (Min, light blue due to laser reflection and DAPI stain). DAPI staining and abundant remains of photosynthetic pigments are visible in the calcite aggregate, showing that diatoms get massively entombed. **E)** Resin-embedded sample also stained with calcein and DAPI. Note the completely cemented subspherical aggregate (dotted line), red diatom pigments (Diat.), and blue cell remains (star).

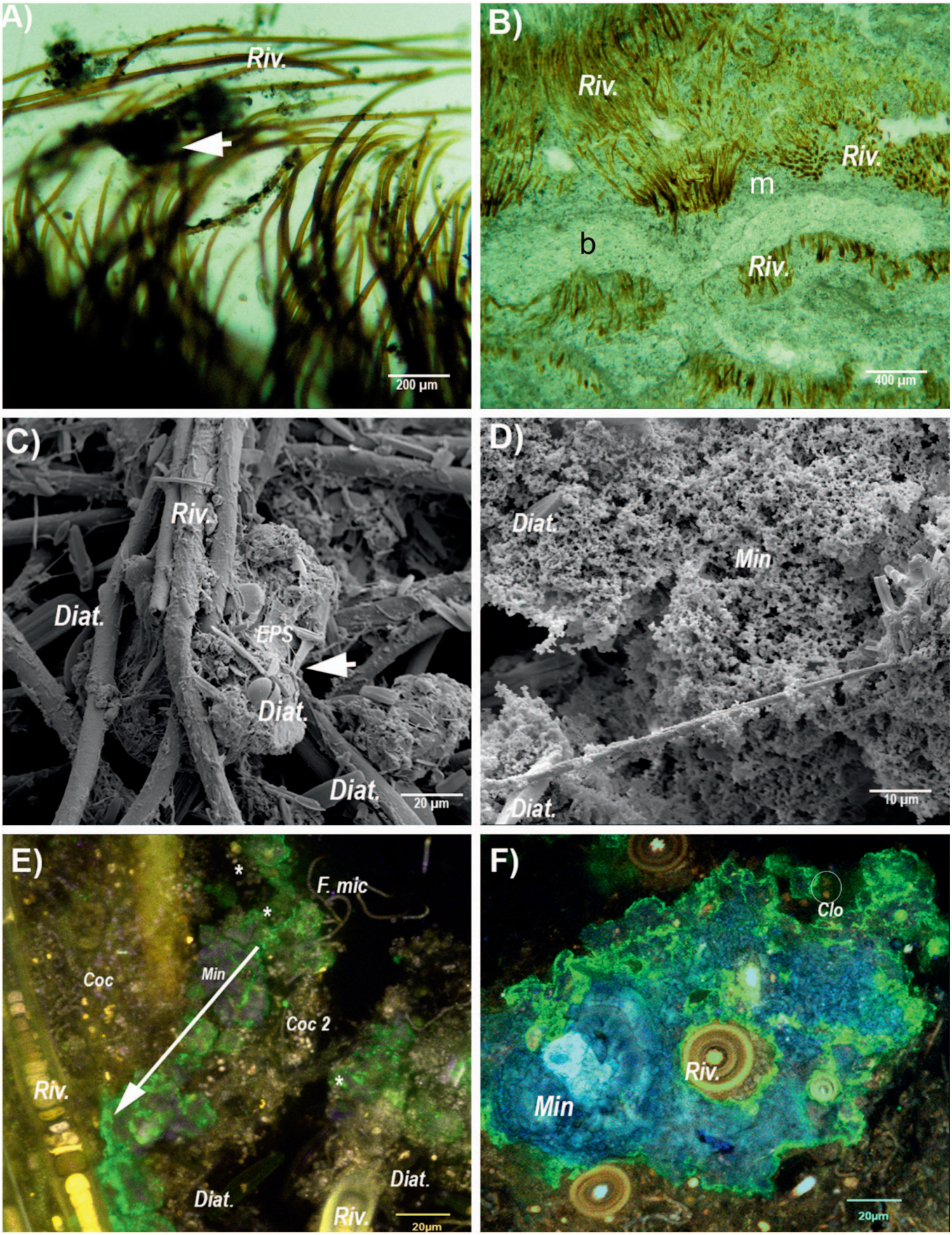
A)
Riv.
200 µm
B)
Riv.
Riv.
m
b
Riv.
400 µm
C)
Riv.
Diat.
EPS
Diat.
Diat.
20 µm
D)
Diat.
Min
Diat.
10 µm
E)
*
F. mic
*
Coc
Min
Coc 2
*
Riv.
Diat.
Diat.
Riv.
20µm
F)
Clo
Riv.
Min
20µm

TABLE 3.—*Microbial-mat carbonates recorded in black pustular, soft greenish, and stratified microbial mats as well as those recorded during diatom blooming events. It is interesting to point out that typically most mats have similar globular to subpherical calcite particles precipitating inside EPS but the carbonates related to diatom blooms are typically aragonite (magnesium calcite present but subordinate) where EPS are absent, suggesting different precipitation mechanisms.*

Microbial Mat Type	Observed Carbonate Textures
Stratified (LN2)	Nano-globular carbonate particles (spherulite-like calcite) less than 500 nm in diameter and located inside the EPS matrix. These are found as part of diatom–microbes aggregates with diameters ranging between 50 and 200 μm (Fig. 5).
Soft greenish (LN9)	Carbonate precipitation inside spherical to slightly elongated calcite aggregates (40–100 μm diameter). Nano-globular carbonate particles occasionally coalesce to form aggregates up to 500 nm. More irregular subhedral particles are also present (Fig. 7).
Black pustular (LN5)	Anhedral, nanometer-size globular to spherical calcite particles (250 nm inside aggregates up to 100 μm diameter. Small size, grumulouse irregular aggregates are also present. Occasionally cyanobacteria (*Rivularia*-like) filaments are encrusted, but carbonates are more typically inside the EPS matrix (Fig. 8).
Pennate-diatom blooms	Euhedral to subhedral aragonite and calcite crystals, typically needles 2 μm long and 0.2 μm wide. More irregular euhedral to subhedral crystals are also present (Fig. 6). These carbonates are associated with oriented pennate diatoms (Fig. 6). Carbonates associated with the pennate-diatoms blooms are not visibly associated with EPS, and that is a main difference with the stratified, greenish, and black pustular mats.

and Défarge 2005; Braissant et al. 2007; Urbani et al. 2012; Underwood 2010), composed of carbohydrates with negatively charged groups (such as uronic acids, sulfated sugars and ketal-linked pyruvate groups, Sutherland 1999a, 1999b; Decho 2010). EPSs produced by marine diatoms are composed of rhamnose, fucose, xylose, mannose, galactose, and glucose (Urbani et al. 2012; Underwood 2010). All these negatively charged EPS can fix cations like Ca^{2+} and Mg^{2+}, and numerous studies have linked EPS production and degradation to carbonate precipitation in both modern and ancient carbonate microbialites (see a review in Visscher and Stolz 2005).

It is known that EPS locally concentrates Ca^{2+} ions, and these are later released during degradation by heterotrophic bacteria and/or physico-chemical degradation (for example, UV radiation or changes in pH). Together with microbial metabolic activity, this results in increased local supersaturation and carbonate precipitation (Decho 2005; Dupraz and Visscher 2005; Braissant et al. 2007, 2009).

Our 16SrDNA studies have shown that heterotrophic saccharolytic bacteria like *Rhodothermaceae*, *Spirochaetaceae*, and *Deinococcaceae*, as well as sulfate-reducing bacteria, are all well represented in the Laguna Negra microbial mats. These bacteria are present and are able to degrade either carbohydrates (Makarova et al. 2007; Park et al. 2014; Karami et al. 2014), proteins, or more complex organic compounds (McIlroy and Nielsen 2014). This, together with the carbonate textural evidence shown in this study (anhedral carbonates spatially associated with the EPS matrix; Table 3, Figs. 5, 7), suggests that microbial EPS degradation and the release of Ca^{2+} and dissolved inorganic carbon (cf. Braissant et al. 2009) could be a carbonate precipitation mechanism inside the Laguna Negra microbial aggregates. The abundance of diatoms and cyanobacteria detected in this work by microscopy and 16SrDNA studies can also increase the pH due to their photosynthetic activity (Riebesell 2000; Arp et al. 2001), driving carbonate equilibrium to favor carbonate precipitation in the mat.

Experimental work has suggested that, in addition to cyanobacteria (Bundeleva et al. 2014) and sulfate-reducing bacteria (Vasconcelos et al. 1995; Bosak and Newman 2003, 2005), purple-sulfur bacteria (PSB) can trigger carbonate precipitation as well as dissolution, and this depends on the environmental conditions (Bundeleva et al. 2012). In our work, the presence of PSB (*Chromatiales* order) has been detected by microscopy and 16SrDNA studies (Fig. 9). Abundant carbonate precipitation spatially associated with these PSB has been observed by CSLM (Fig. 5G) suggesting some possible influence on carbonate precipitation as well. Thus, the precipitation of carbonates will depend on the net balance of microorganisms bearing different metabolisms (Visscher and Stolz 2005).

EPSs are known to control carbonate nucleation (Giuffre et al. 2013; Hamma et al. 2014), crystal morphology, and carbonate polymorphs (Kawaguchi and Decho 2002; Braissant et al. 2003; Chekroun et al. 2004; Wang et al. 2012). The prevalence of anhedral, spherulitic, and globular carbonate nano-particles in the Laguna Negra microbial mats (Table 3) suggests that these precipitated under the influence of an EPS matrix, where EPS controls carbonate nucleation and crystal growth. In modern and ancient carbonate microbialites, irregular micrite laminae composed of nano-globular carbonates are considered to be produced by precipitation related to organic polymers and with strong biological influence (Trichet

←

FIG. 8.—Images of microorganisms associated with the Black Pustular mat in Laguna Negra. **A)** BP mat sample observed under optical microscopy: abundant *Rivularia*-like filaments (Riv.) are visible. The white arrow indicates irregular aggregates of microorganisms and minerals attached to those filaments. **B)** Thin section of an oncoid sample showing the paintbrush-like palisade fabric of *Rivularia*-like filaments encrusted by carbonates and preserved alternating with other lamina types like sparry botryoidal (sb) and micritic (m), inside oncoids that occasionally are colonized by the black pustular mat. **C)** SEM image of *Rivularia* (Riv) filaments in the BP mat showing that abundant diatom frustules (Diat.) and EPS are visible on the surface of the mineral aggregate (white arrow). **D)** Closer view showing the nano-globular texture of calcite (Min) in the aggregates, several encrusted diatom frustules (Diat.) are visible. E, F) Composite three-color CLSM image of a resin-embedded cross-sectioned microbialite stained with calcein and DAPI obtained with a concomitant excitation at wavelengths of 405 nm, 488 nm, and 543 nm. **E)** The shiny orange-red fluorescence in the *Rivularia*-like filaments corresponds to residual fluorescence of photosynthetic pigments partially preserved through the embedding process. The blue fluorescence corresponds to DAPI staining of DNA in the cells, allowing detection of abundant cocci (Coc) and filamentous microbial cells around the *Rivularia*-like filaments. Some of those unidentified coccoid cells are autofluorescent, appearing as pink to shiny orange-red dots (Coc 2), suggesting that some of those cocci include fluorescent pigments. Calcein staining is visible in green, highlighting accessible Ca^{2+} at the surface of the mat associated with the fluorescent cocci cells and around the calcite grains (purple-blue). Mineral grains (Min) appear in purple-blue due to laser reflection, residual entombed microbial pigments as well as stained DNA and DAPI fixation on minerals. Mineral precipitation seems to begin in unidentified coccoid cells at the top of the mat (white stars). The white arrow indicates the increasing size of the mineral grains from the surface to the depth of the microbial mat leading to the progressive entombment of the *Rivularia*-like filaments. **F)** Cross section of Rivularia-like filaments, surrounded by minerals (carbonates in light blue surrounded by calcein staining in green) showing the progressive entombment of the *Rivularia*-like filaments. Some residual diatom chloroplasts (Clo) are also detected in the mineralized zone.

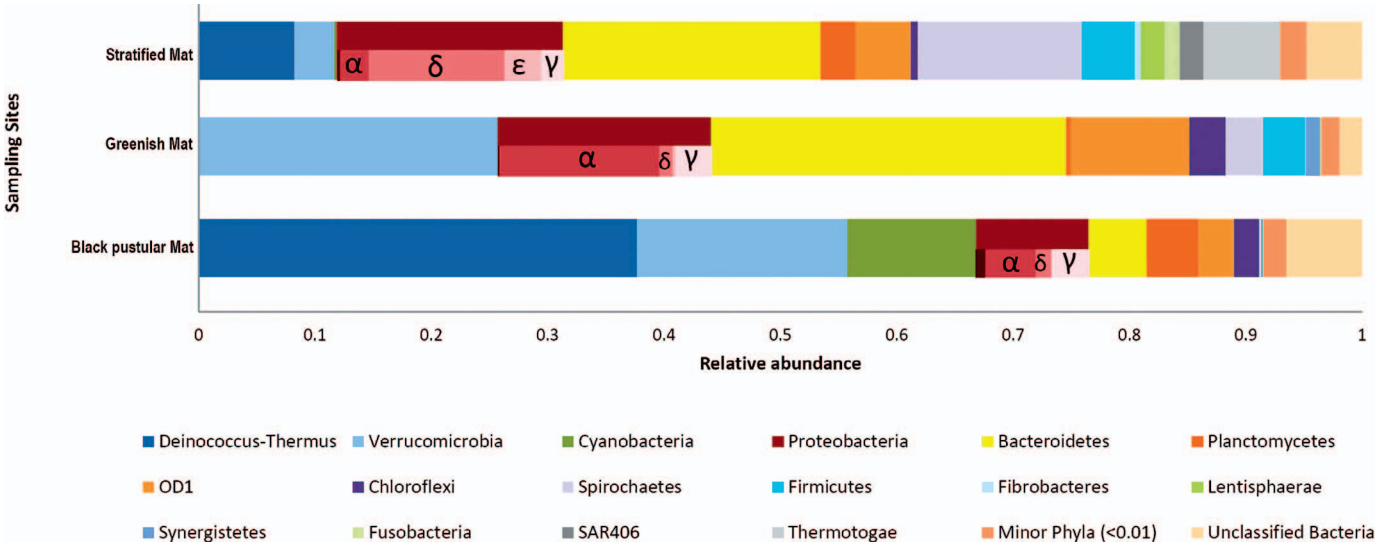

FIG. 9.—Relative abundance of Phylum-level community composition derived from each sampling site. Category "Minor Phyla (< 0.01)" includes among the classified phyla, Acidobacteria, Actinobacteria, Armatinmonadetes, Chlamydiae, Chlorobi, Gemmatimonadetes, and Tenericutes. Within the Proteobacteria, alpha (α) indicates Alphaproteobacteria, delta (δ) Deltaproteobacteria, gamma (γ) Gammaproteobacteria, and epsilon (ε) Epsilonproteobacteria.

and Defárge 1995; Defárge 2010; Riding 2008, 2011), and the same is found for the Laguna Negra (Gomez et al. 2014; this study) (Tables 1, 3).

Carbonate Precipitation not Associated with EPS

It is worth noting the record of localized spontaneous mineral precipitation events (whitings) inside the microbial ponds (pink to orange mats), which are related to pennate-diatom blooms (Fig. 6A). These carbonates are almost exclusively subhedral to euhedral aragonite and calcite (Figs. 6B, D). They are texturally and mineralogically different (aragonite needles versus nanoglobular calcite, Table 1) when compared with most of the carbonates precipitated inside the EPS matrix in the microbial mat aggregates, suggesting a different mechanism. In the particular case of pennate-diatom blooming events, we suggest that the EPS influence was marginal or absent. Diatoms assimilate CO_2 through assimilation of HCO_3^- (Riebesell 2000), producing OH^- and increasing the pH. This increases carbonate-ion concentration and together with calcium can promote calcium carbonate saturation and precipitation. The lack of EPS favors the development of euhedral aragonite needles. High Mg^{2+} concentration is known to favor aragonite precipitation, which usually occurs when the Mg/Ca ratio is above 1.1 (Rossi and Lozano 2016) or 2 (Sun et al. 2015; Jones 2017), which is not the case in the Laguna Negra (Gomez et al. 2014), that potentially suggests some biological influence. Similar aragonite precipitation formed under biological influence has been documented during whiting events, triggered by picoplankton blooming (Sondi and Juračić 2010), although the controls are still poorly understood.

This precipitation of aragonite during diatom blooms first occurs in the pond water column (a few centimeters deep), but then the aragonite and diatoms settle into the substrate (Fig. 6A). This provides a site for further carbonate nucleation, lamina accretion, and development of some of the Laguna Negra oncoids. This is supported by the observation that remarkably similar laminae with parallel-oriented diatoms (*Nitzschia* sp.) have been recorded in some oncoids (Fig. 6E).

CONCLUDING REMARKS

Diatom–bacteria aggregates represent an important component in the Laguna Negra microbial mats. Diatom–bacteria aggregation and interaction impact the preserved microbialite textures and fabrics. Environmental conditions may have controlled diatom aggregation, given the abundant EPS production and the capacity of EPS to fix cations like Ca^{2+}, inducing aggregation. SEM and CLSM studies revealed that most carbonate precipitation has been related to the EPS matrix in the observed diatom–bacteria aggregates. As shown by bacterial 16rDNA and microscopy studies, these aggregates preserved a complex microbial community including diatoms, coccoid and filamentous cyanobacteria, and purple sulfur bacteria. The abundance of diatoms in the Laguna Negra microbial mats may play a central role in EPS production. In addition there is an abundance of heterotrophic saccharolytic groups that are able to degrade EPS. Our results suggest that the interactions between diatoms and bacteria inside these aggregates, including photosynthetic activity (locally increasing pH by releasing OH^-), and heterotrophic activity (degrading EPS making Ca^{2+} available) create microenvironments favorable for carbonate precipitation. The EPS-related precipitates show textures and fabrics that contrast markedly with those carbonates precipitated without EPS influence. Texturally and mineralogically different carbonates (aragonite needles) are observed when EPS are absent, such as the case of pennate-diatom blooming events. Other bacteria groups, like purple-sulfur bacteria and sulfate-reducing bacteria, recorded inside the diatom–bacteria aggregates, are spatially associated with carbonate mineral, and thus could also have influenced carbonate precipitation.

Different carbonate-laminae types observed in the oncoidal microbialites record changes in microbial communities, interpreted to be triggered by environmental changes. For example, when subaqueous oncoids develop in the pink stratified mats, they form white granular diatom-rich carbonates. Alternatively, when oncoids are partially exposed, the black pustular mat colonizes areas close to the air–water interface and this is preserved as lamina with calcified *Rivularia*-like filaments with tufted, palisade fabrics (Table 1). While previous work has suggested that physicochemical processes, such as water mixing, evaporation, and CO_2 degassing, may act as potential carbonate-precipitation triggers (Gomez et al. 2014), this work indicates that microbial activity influences the location, textures, and fabrics of the precipitated calcite and aragonite.

Abundant EPS production by these diatom-rich microbial mats could be a mechanism to prevent cell-frustule entombment in this rapidly mineralizing setting. EPS production can be a response to environmental stress related to desiccation, high UV influx, and nutrient availability and

salinity, to cope with the extreme environmental conditions that characterize the Laguna Negra system. Carbonate precipitation inside diatom-rich microbial mats and during diatom blooming events highlights the potential for diatoms to rapidly precipitate carbonates and their potential role in microbialite formation. The contrast between microbialites developed before and after diatoms appear in the geological record demands further study.

SUPPLEMENTAL MATERIAL

Figures S1 and S2 and Table S1 are available from JSR's Data Archive: https://www.sepm.org/JSR-Data-Archive.

ACKNOWLEDGMENTS

Funding and support was provided by the NASA (National Aeronautics and Space Administration) Planetary Biology Internship Program (F.J.G.), the Fulbright Program (F.J.G. and F.B.), the Houssay Grant Program (C.M.), the CICTERRA (Centro de Investigaciones en Ciencias de la Tierra), the ANPCyT (Agencia Nacional de Promoción de Ciencia y Técnica), the CONICET (Consejo Nacional de Investigaciones Científicas y Técnicas) (International Cooperation Program, CONICET, Institut de Physique du Globe de Paris), projects PICT-1306 (F.J.G.) and PICT-1788 (F.J.G. and M.E.F.), and the SECYT (Secretaria de Ciencia y Técnica, Universidad Nacional de Córdoba), Project 214/10-11. We appreciate comments made by two anonymous reviewers and the associate editors which significantly improved this manuscript. We thank Daniel Kurth (LIMLA, Tucumán, Argentina) for assistance in sequences processing and Dr. Noemi Gari (Dpto. Cs. Naturales Fac. Ciencias Exactas, Fco-Qcas. y Naturales, UNRC) for diatom identification. We thank Luciano Montoya and Martin Argota for field assistance and Wendy Walker for her help reviewing English grammar and style. We want to acknowledge that this research was also supported by the Catamarca Province Environmental Agency (Mr. Luis Costantini, Gobernación de la Provincia de Catamarca Secretaría de Estado del Ambiente y Desarrollo Sustentable, Dirección Provincial de Gestión Ambiental). F.J.G. also wants to acknowledge to the Internacional Geobiology Course Team and the USC Wrigley Institute for Environmental Studies for the continuous work to promote and develop Geobiology research. This is IPGP contribution number 3945.

REFERENCES

Allwood, A., Walter, M., Kamber, B., and Burch, I., 2006, Stromatolite reef from the early Archaean era of Australia: Nature, v. 441, p. 714–718.

Amin, S., Parker, M., and Armbrust, E., 2012, Interactions between diatoms and bacteria: Microbiology and Molecular Biology Reviews, v. 76, p. 667–684.

Arp, G., Reimer, A., and Reitner, J., 1999, Calcification in cyanobacterial biofilms of alkaline salt lakes: European Journal of Phycology, v. 34, p. 393–403.

Arp, G., Reimer, A., and Reitner, J., 2001, Photosynthesis-induced biofilm calcification and calcium concentrations in the Phanerozoic oceans: Science, v. 292, p. 1701–1704.

Awramik, S., and Riding, R., 1988, Role of algal eukaryotes in subtidal columnar stromatolite formation: National Academy of Sciences (USA), Proceedings, v. 85, p. 1327–1329.

Bellinger, B., Abdullahi, A., Gretz, M., and Underwood, G., 2005, Biofilm polymers: relationship between carbohydrate biopolymers from estuarine mudflats and unialgal cultures of benthic diatoms: Aquatic Microbial Ecology, v. 38, p. 169–180.

Banfield, J., Moreau, J., Chan, C., Welch, S., and Little, B., 2001, Mineralogical biosignatures and the search for life on mars: Astrobiology, v. 1, p. 447–465.

Bosak, T., and Newman, D., 2003, Microbial nucleation of calcium carbonate in the Precambrian: Geology, v. 31, p. 577–580.

Bosak, T., and Newman, D., 2005, Microbial kinetic controls on calcite morphology in supersaturated solutions: Journal of Sedimentary Research, v. 75, p. 190–199.

Bosak, T., Greene, S., and Newman, D., 2007, Anoxygenic photosynthetic bacteria and calcite crusts a likely role for anoxygenic photosynthetic microbes in the formation of ancient stromatolites: Geobiology, v. 5, p. 119–126.

Braissant, O., Cailleau, G., Dupraz, C., and Verrecchia, E., 2003, Bacterially induced mineralization of calcium carbonate in terrestrial environments: the role of exopolysaccharides and amino acids: Journal of Sedimentary Research, v. 73, p. 485–490.

Braissant, O., Decho, A., Dupraz, C., Glunk, C., Przekop, K., and Visscher, P., 2007, Exopolymeric substances of sulfate-reducing bacteria: interactions with calcium at alkaline pH and implication for formation of carbonate minerals: Geobiology, v. 5, p. 401–411.

Braissant, O., Decho, A.W., Przekop, K.M., Gallagher, K.L., Glunk, C., Dupraz, C., and Visscher, P.T., 2009, Characteristics and turnover of exopolymeric substances in a hypersaline microbial mat: Federation of European Microbiological Societies, Microbiology Ecology, p. 67, p. 293–307.

Brehm, U., Krumbein, W.E., and Palinska, K.A., 2004, Laboratory cultures of calcifying biomicrospheres generate ooids: a contribution to the origin of oolites: Carnets de Geologie, Notebooks on Geology, Letter 2004/03 (CG2003_L03).

Brehm, U., Krumbein, W.E., and Palinska, K.A., 2006, Biomicrospheres generate ooids in the laboratory: Geomicrobiology Journal, v. 23, p. 545–550.

Brinkmann, N., Hodač, L., Mohr, K., Hodačová, A., Jahn, R., Ramm, J., Hallmann, C., Arp, G., and Friedl, T., 2015, Cyanobacteria and diatoms in biofilms of two karstic streams in Germany and changes of their communities along calcite saturation gradients: Geomicrobiology Journal, v. 32, p. 255–274.

Buck, K., and Chavez, F., 1994, Diatom aggregates from the open ocean: Journal of Plankton Research, v. 16, p. 1449–1457.

Bundeleva, I., Shirokova, L., Bénézeth, P., Pokrovskya, O., Kompantseva, E., and Balor, S., 2012, Calcium carbonate precipitation by anoxygenic phototrophic bacteria: Chemical Geology, v. 291, p. 116–131.

Bundeleva, I., Shirokova, L., Bénézeth, P., Pokrovskya, O., Kompantseva, E., Balor, S., Menez, B., and Gérard, E., 2014, Experimental modeling of calcium carbonate precipitation by cyanobacterium *Gloeocapsa* sp: Chemical Geology, v. 274–275, p. 44–60.

Buongiorno, J., 2014, Mineralized microbialites as archives of environmental evolution of a hypersaline lake basin: Laguna Negra, Catamarca Province, Argentina [Master's thesis]: University of Tennessee, Knoxville, 231 p.

Burne, R., and Moore, L., 1987, Microbialites: organosedimentary deposits of benthic microbial communities: Palaios, v. 2, p. 241–254.

Canfield, D., Habicht, K., and Thamdrup, B., 2000, The Archean sulfur cycle and the early history of atmospheric oxygen: Science, v. 288, p. 658–661.

Canfield, D., Rosing, M., and Bjerrum, C., 2006, Early anaerobic metabolisms: Royal Society of London, Philosophical Transactions B, Biological Sciences, v. 361, p. 1819–1836.

Caporaso, J.G., Kuczynski, J., Stombaugh, J., Bittinger, K., Bushman, F.D., Costello, E.K., Fierer, N., Pena, A.G., Goodrich, J.K., Gordon, J.I., Huttley, G.A., Kelley, S.T., Knights, D., Koenig, J.E., Ley, R.E., Lozupone, C.A., McDonald, D., Muegge, B.D., Pirrung, M., Reeder, J., Sevinsky, J.R., Turnbaugh, P.J., Walters, W.A., Widmann, J., Yatsunenko, T., Zaneveld, J., and Knight, R., 2010, QIIME allows analysis of high-throughput community sequencing data: Nature Methods, v. 7, p. 335–336.

Catling, D., and Claire, M., 2005, How Earth's atmosphere evolved to an oxic state: a status report: Earth and Planetary Science Letters, v. 237, p. 1–20.

Chekroun, B.K., Rodriguez-Navarro, C., Gonzalez-Munoz, M.T., Arias, J.M., Cultrone, G., and Rodriguez-Gallego, M., 2004, Precipitation and growth of calcium carbonate induced by *Myxococcusxanthus*: implication for recognition of bacterial carbonates: Journal of Sedimentary Research, v. 74, p. 868–876.

Cooksey, K.E., 1981, Requirement for calcium in adhesion of a fouling diatom to glass: Applied Environmental Microbiology, v. 41, p. 1378–1382.

Decho, A., 2010, Overview of biopolymer-induced mineralization: what goes on in biofilms?: Ecological Engineering, v. 36, p. 137–144.

Défargue, C., 2010, Organomineralization, *in* Reitner, J., and Thiel, V., eds., Encyclopedia of Geobiology: Berlin, Springer, p. 697–701.

Dittrich, M., and Obst, M., 2004, Are picoplankton responsible for calcite precipitation in lakes? AMBIO: A Journal of the Human Environment, v. 33, p. 559–564.

Dittrich, M., and Sibler, S., 2010, Calcium carbonate precipitation by cyanobacterial polysaccharides, *in* Pedley, H.M., and Rogerson, M., eds., Tufas and Speleothems: Unravelling Microbial and Physical Controls: Geological Society of London, Special Publication 336, p. 51–63.

Douglas S., 2005, Mineralogical footprints of microbial life: American Journal of Science, v. 305, p. 503–525.

Dupraz, C., and Visscher, P., 2005, Microbial lithification in marine stromatolites and hypersaline mats: Trends in Microbiology, v. 13, p. 429–438.

Falkowski, P., Fenchel, T., and Delong, E., 2008, The microbial engines that drive Earth's biogeochemical cycles: Science, v. 320, p. 1034–1039.

Farías, M.E., Rascovan, N., Toneatti, D., Albarracín, V., Flores, M.R., Ordoñez, O., Poiré, D.G., Collavino, M., Aguilar, O., Vazquez, M., and Polerecky, L., 2013, The discovery of stromatolites developing at 3570 m above sea level in a high-altitude volcanic Lake Socompa, Argentinean Andes: PLoS ONE, v. 8, p. 1–15.

Farías, M.E., Contreras, M., Rasuk, M.D., Kurth, D., Flores, M.R., Poiré, D.G., Novoa, F., and Visscher, P.T., 2014, Characterization of bacterial diversity associated with microbial mats, gypsum evaporites and carbonate microbialites in thalassic wetlands: Tebenquiche and La Brava, Salar de Atacama, Chile: Extremophiles, v. 18, p. 301–329.

Fernandez, A.B., Rasuk, M.C., Visscher, P.T., Contreras, M., Novoa, F., Poire, D., Patterson, M.M., Ventosa, A., and Farias, M.E., 2016, Microbial diversity in sediment ecosystems (evaporite domes, microbial mats and crusts) of hypersaline Laguna Tebenquiche, Salar de Atacama, Chile: Frontiers in Microbiology, Extreme Microbiology, v. 7, doi: 10.3389/fmicb.2016.01284.

Garcia-Pichel, F., and Castenholz, R., 1994, Characterization and biological implications of scytonemin, a cyanobacterial sheath pigment: Journal of Phycology, v. 27, p. 395–409.

Garcia-Pichel, F., Al-Horani, F., Farmer, J., Rebecca, L., and Wade, B., 2004, Balance between microbial calcification and metazoan bioerosion in modern stromatolitic oncolites: Geobiology, v. 2, p. 45–57.

Gérard, E., Ménez, B., Couradeau, E., Moreira, D., Benzerara, K., Tavera, R., and López-García, P., 2013, Specific carbonate–microbe interactions in the modern microbialites of Lake Alchichica (Mexico): The International Society for Microbial Ecology, Journal, v.7, p. 1997–2009.

Giuffre, A., Hamma, L., Hana, N., DeYoreo, J., and Dove, P., 2013, Polysaccharide chemistry regulates kinetics of calcite nucleation through competition of interfacial energies: National Academy of Sciences (USA), Proceedings, v. 110, p. 9261–9266.

Gomez, F.J., Kah, L., Bartley, J., and Astini, R., 2014, Microbialites in a high altitude Andean lake: multiple controls on carbonate precipitation and lamina accretion: Palaios, v. 29, p. 233–249.

Gonzalez-Muñoz, M., Chekroun, B.K., Aboud, A., Arias, J.M., and Rodriguez-Gallego, M., 2000, Bacterially induced Mg-calcite formation: role of Mg^{2+} in development of crystal morphology: Journal of Sedimentary Research, v. 70, p. 559–564.

Hamma, L., Giuffre, A., Hana, N., Tao, J., Wang, D., Yoreo, J., and Dove, P., 2014, Reconciling disparate views of template-directed nucleation through measurement of calcite nucleation kinetics and binding energies: National Academy of Sciences (USA), Proceedings, v. 111, p. 1304–1309.

Herman, E., and Kump, L., 2005, Biogeochemistry of microbial mats under Precambrian oceanic conditions: a modeling study: Geobiology, v. 3, p. 77–92.

Hoagland, K., Rosowski, J., Gretz, M., and Roemer, S., 1993, Diatoms extracellular polymeric substances: function, fine structure, chemistry and physiology: Journal of Phycology, v. 29, p. 537–566.

Jones, B., 2017, Review of calcium carbonate polymorph in spring systems: Sedimentary Geology, v. 353, p. 64–75.

Jones, B., and Renault, R., 1994, Crystal fabrics and microbiota in large pisoliths from Laguna Pastos Grandes: Sedimentology, v. 41, p. 1171–1202.

Jordan, T., and Alonso, R., 1987, Cenozoic stratigraphy and basin tectonics of the Andes mountains, 20–28° south latitude: American Association of Petroleum Geologists, Bulletin, v. 71, p. 49–64.

Kallmeyer, J., Pockalny, R., Adhikari, R., Smith, D., and D'Hondt, S., 2012, Global distribution of microbial abundance and biomass in subseafloor sediment: National Academy of Sciences (USA), Proceedings, v. 109, p. 16213–16216.

Kamennaya, N., Ajo-Franklin, C., Northen, T., and Jansson, C., 2012, Cyanobacteria as biocatalysts for carbonate mineralization: Minerals, v. 2, p. 338–364.

Karami, A., Sarshar, M., Ranjbar, R., and Sorouri Zanjani, R., 2014, The Phylum Spirochaetaceae, *in* Rosenberg, E., DeLong, E.F., Lory, S., Stackebrandt, E., and Thompson, F., eds., The Prokaryotes, Springer, p. 915–929.

Kawaguchi, T., and Decho, A., 2002, A laboratory investigation of cyanobacterial extracellular polymeric secretions (EPS) in influencing $CaCO_3$ polymorphism: Journal of Crystal Growth, v. 240, p. 230–235.

Kenward, P., Goldstein, R., González, L., and Roberts, J., 2009, Precipitation of low-temperature dolomite from an anaerobic microbial consortium: the role of methanogenic Archaea: Geobiology, v. 7, p. 556–565.

Knoll, A., Bergmann, K., and Strauss, J.V., 2016, Life: the first two billion years: Royal Society of London, Philosophical Transactions B, v. 371, p. 1471–20970.

Konhauser, K., 2007, Introduction to Geomicrobiology: Wiley-Blackwell, 440 p.

Makarova, K.S., Omelchenko, M.V., Gaidamakova, E.K., Matrosova, V.Y., Vasilenko, A., Zhai, M., Lapidus, A., Copeland, A., Kim, E., Land, M., Mavrommatis, K., Pitluck, S., Richardson, P.M., Detter, C., Brettin, T., Saunders, E., Lai, B., Ravel, B., Kemner, K.M., Wolf, Y.I., Sorokin, A., Gerasimova, A.V., Gelfand, M.S., Fredrickson, J.K., Koonin, E.V., and Daly, M.J., 2007, Deinococcusgeothermalis: the pool of extreme radiation resistance genes shrink: PLoS ONE, v. 26, e955.

McIlroy, S.J., and Nielsen, P.H., 2014, The Family *Saprospiraceae*, *in* Rosenberg, E., DeLong, E.F., Lory, S., Stackebrandt, E., and Thompson, F., eds., The Prokaryotes, Springer, p. 863–889.

Meister, P., 2013, Two opposing effects of sulfate reduction on calcite and dolomite precipitation in marine, hypersaline and alkaline environments: Geology, v. 41, p. 499–502.

Murray, R., Cooksey, K., and Priscu, J., 1986, Stimulation of bacterial DNA synthesis by algal exudates in attached algal–bacterial consortia: Applied and Environmental Microbiology, p. 52, p. 1177–1182.

Park, S., Akira, Y., and Kogure, K., 2014, The Family *Rhodothermaceae*, *in* Rosenberg, E., DeLong, E.F., Lory, S., Stackebrandt, E., and Thompson, F., eds., The Prokaryotes, Springer, p. 849–856.

Perry, R., Mcloughlin, N., Lynne, B., Sephton, M., Oliver, J., Perry, C., Campbell, K., Engel, M., Farmer, J., Brasier, M., and Staley, J., 2007, Defining biominerals and organominerals: direct and indirect indicators of life: Sedimentary Geology, v. 201, p. 157–179.

Powell, R., and Hill, R., 2014, Mechanism of algal aggregation by Bacillus sp. strain rp1137: Applied and Environmental Microbiology, p. 80, p. 4042–4050.

Rascovan, N., Maldonado, M.J., Vazquez, M.P., and Farías, M.E., 2015, Bioenergetic use of arsenic in haloarchaea biofilms from Diamante Lake: The International Society for Microbial Ecology, Journal, v. 10, p. 299–309.

Rastogi, R., and Incharoensakdi, A., 2014, Characterization of UV-screening compounds, mycosporine-like amino acids, and scytonemin in the cyanobacterium *Lyngbya* sp. cu2555: Federation of European Microbiological Societies, Microbiology Ecology, v. 87, p. 244–256.

Rasuk, M., Kurth, D., Flores, R., Contreras, M., Novoa, F., Poire, D., and Farias, M., 2014, Microbial characterization of a gypsum endoevaporitic ecosystem in Salar de Llamara, Chile: Microbial Ecology, v. 68, p. 483–494.

Rasuk, M., Fernández, A., Kurth, D., Contreras, M., Novoa, F., Poiré, D., and Farías, M.E., 2015, Bacterial diversity in microbial mats and sediments from the Atacama Desert: Microbial Ecology, v. 71, p. 44–56.

Riding, R., 2008, Abiogenic, microbial and hybrid authigenic carbonate crusts: components of Precambrian stromatolites: Geologica Croatica, v. 61, p. 73–103.

Riding, R., 2011, The nature of Stromatolites: 3500 million years of history and a century of research, *in* Reitner, J., Quéric, N.V., and Arp, G., eds., Advances in Stromatolite Geobiology: Berlin, Springer-Verlag, Lecture Notes in Earth Sciences, v. 131, p. 29–74.

Riebesell, U., 1991, Particle aggregation during a diatom bloom II: biological aspects: Marine Ecology, Progress Series, v. 69, p. 281–291.

Riebesell, U., 2000, Photosynthesis: carbon fix for a diatom: Nature, v. 407, p. 959–960.

Risacher, F., and Eugster, H., 1979, Holocene pisolites and encrustations associated with spring-fed surface pools, Pastos Grandes, Bolivia: Sedimentology, v. 26, p. 253–270.

Rossi, C., and Lozano, R.P., 2016, Hydrochemical controls on aragonite versus calcite precipitation in cave dripwaters: Geochimica et Cosmochimica Acta, v. 192, p. 70–96.

Schrag, D., Higgins, J.A, McDonald, F.A., and Johnston, D., 2013, Authigenic carbonate and the history of the global carbon cycle: Science, v. 339, p. 540–543.

Soetaert, K., Hofmann, A.F., Middelburg, J.J., Meysman, F.J.R, and Greenwood, J., 2007, The effect of biogeochemical processes on pH: Marine Chemistry, v. 106, p. 380–401.

Sondi, I., and Juračić, M., 2010, Whiting events and the formation of aragonite in Mediterranean karstic marine lakes: new evidence on its biologically induced inorganic origin: Sedimentology, v. 57, p. 85–95.

Stal, L., and Défarge, C., 2005, Structure and dynamics of exopolymersin an intertidal diatom biofilm: Geomicrobiology Journal, v. 22, p. 341–352.

Sun, I., Saivenkataraman, J., and Chen, W., Persson K.A., and Gerbran, C., 2015, Nucleation of metastable aragonite $CaCO_3$ in seawater: National Academy of Sciences (USA), Proceedings, v. 112, p. 3199–3204.

Sutherland, I., 1999a, Polysaccharases for microbial polysaccharides: Carbohydrate Polymers, v. 38, p. 319–328.

Sutherland, I., 1999b, Polysaccharases in biofilms: sources, action and consequences, *in* Wingender, J., Neu, T.R., and Flemming, H.C., eds., Microbial Extracellular Polymeric Substances: Characterization, Structure and Function: Berlin, Springer, p. 201–216.

Teske, A., and Stahl, D., 2002, Microbial mats and biofilms: evolution, structure and function of fixed microbial communities, *in* Stanley, J.T., and Reysenbach, A.L., eds., Biodiversity of Microbial Life: Foundations of Earth's Biosphere, New York, John Wiley, p. 49–100.

Thompson, J., Schultze-Lam, S., Beveridge, T., and DesMarais, D., 1997, Whiting events: biogenic origin due to the photosynthetic activity of cyanobacterial picoplankton: Limnology and Oceanography, v. 42, p. 133–141.

Thornton, D.C.O., 2002, Diatom aggregation in the sea: mechanisms and ecological implications: European Journal of Phycology, v. 37, p. 149–161.

Trichet, J., and Defârge, C., 1995, Non-biologically supported organomineralization: Institute Océanographique de Monaco, Bulletin, v. 14, p. 203–236.

Underwood, G., 2010, Exopolymers (extracellular polymeric substances) in diatom-dominated marine sediment biofilms, *in* Seckbach, J., and Oren, A., eds., Cellular Origin, Life in Extreme Habitats and Astrobiology, p. 287–300, the Netherlands, Springer.

Urbani, R., Sist, P., Pletikapić, G., Radić, T.M., Svetličić, V., and Žutic, V., 2012, Diatom polysaccharides: extracellular production, isolation and molecular characterization, *in* Karunaratne, D.N., ed., The Complex World of Polysaccharides: INTECH, Croatia, http://dx.doi.org/10.5772/51251.

Valero-Garcés, B., Delgado-Huertas, A., Ratto, N., Navas, A., and Edwards, L., 2000, Paleohydrology of Andean saline lakes from sedimentological and isotopic records, northwestern Argentina: Journal of Paleolimnology, v. 24, p. 343–359.

Vandervoort, D., Jordan, T., Zeitler, P., and Alonso, R., 1995, Chronology of internal drainage development and uplift, southern Puna plateau, Argentine Central Andes: Geology, v. 23, p. 145–148.

Vasconcelos, C., McKenzie, J., Bernaconi, S., Grujic, D., and Tien, A., 1995, Microbial mediation as a possible mechanism for natural dolomite formation at low temperatures: Nature, v. 377, p. 220–222.

Visscher, P., and Stolz, J., 2005, Microbial mats as bioreactors: populations, processes, and products: Palaeogeography, Palaeoclimatology, Palaeoecology, v. 219, p. 87–100.

Wade, B., and Garcia-Pichel, F., 2003, Evaluation of DNA extraction methods for molecular analysis of microbial communities in modern calcareous microbialites: Geomicrobiology Journal, v. 20, p. 549–561.

Waksman, S.A., Stokes, J.L., and Butler, M.R., 1937, Relation of bacteria to diatoms in sea water: Marine Biological Association of the United Kingdom, Journal, v. 22, p. 359–373.

Wang, D., Hamm, L., Giuffre, A., Echigo, T., Rimstidt, J., DeYoreo, J., Grotzinger, J., and Dove, P., 2012, Revisiting geochemical controls on patterns of carbonate deposition through the lens of multiple pathways to mineralization: Faraday Discussions, v. 159, p. 371–386.

Whitman, W., Coleman, D., William, J., and Wiebe, W., 1998, Prokaryotes: the unseen majority: National Academy of Sciences (USA), Proceedings, v. 95, p. 6578–6583.

Winsborough, B., 2000, Diatoms and benthic microbial carbonates, *in* Riding, R.E., and Awramik, S.M., eds., Microbial Sediments: Berlin, Springer, p. 76–83.

Winsborough, B., and Golubic, S., 1987, The role of diatoms in stromatolite growth: two examples from modern freshwater settings: Journal of Phycology, v. 23, p. 195–201.

Zeng, Z., and Tice, M., 2014, Promotion and nucleation of carbonate precipitation during microbial iron reduction: Geobiology, v. 12, p. 362–371.

Received 14 February 2017; accepted 29 March 2018.